Crustal and Upper Mantle Imaging of Botswana Using Magnetotelluric Method

Stephen Akinremi[1], Islam Fadel[1], and Mark van der Meijde[1]

[1]University of Twente - Faculty of ITC

November 24, 2022

Abstract

We used magnetotelluric data from 352 sites in Botswana to derive a nationwide electrical conductivity model of the crust and upper mantle structure. A robust methodological scheme and 3D inversion were used to derive a 3D electrical conductivity model with unprecedented spatial coverage. The model results show interesting features, including the major cratonic blocks and the mobile belts in Botswana. A distinctive resistive structure was imaged in southwest Botswana, which suggests the existence of the Maltahohe microcraton as a separate cratonic unit as proposed by other studies. Furthermore, the model gives new insight into the extension of the East African Rift System to Botswana and the incipient rifting in the Okavango Rift Zone. In northern Botswana, the electrical conductivity model shows a high conductivity structure beneath the Okavango Rift Zone, which connects with a deeper high conductivity structure that we attribute to the East African Rift System due to its vicinity to Lake Kariba, the last surface expression of the rift system. We suggest that ascending fluids or melt from the East African Rift System causes the weakening of the lithosphere and plays a significant role in the incipient continental rifting in the Okavango Rift Zone.

Crustal and Upper Mantle Imaging of Botswana Using Magnetotelluric Method

Stephen Akinremi[1*], Islam Fadel[1], Mark van der Meijde[1]

[1]Faculty of Geo-Information Science and Earth Observation (ITC), University of Twente, Enschede, The Netherlands.

*** Correspondence:**
Stephen Akinremi
s.akinremi@utwente.nl

Keywords: Electrical modelling, Magnetotellurics, Tectonics, Continental Rift, Rift Initiation, Africa.

Number of Words: 8934

Number of Figures: 6

Number of Table: None

Abstract

We used magnetotelluric data from 352 sites in Botswana to derive a nationwide electrical conductivity model of the crust and upper mantle structure. A robust methodological scheme and 3D inversion were used to derive a 3D electrical conductivity model with unprecedented spatial coverage. The model results show interesting features, including the major cratonic blocks and the mobile belts in Botswana. A distinctive resistive structure was imaged in southwest Botswana, which suggests the existence of the Maltahohe microcraton as a separate cratonic unit as proposed by other studies. Furthermore, the model gives new insight into the extension of the East African Rift System to Botswana and the incipient rifting in the Okavango Rift Zone. In northern Botswana, the electrical conductivity model shows a high conductivity structure beneath the Okavango Rift Zone, which connects with a deeper high conductivity structure that we attribute to the East African Rift System due to its vicinity to Lake Kariba, the last surface expression of the rift system. We suggest that ascending fluids or melt from the East African Rift System causes the weakening of the lithosphere and plays a significant role in the incipient continental rifting in the Okavango Rift Zone.

1. Introduction

Our understanding of the geology and tectonics of Botswana still carry a few disputed and debated hypotheses. Botswana has a diverse geology with large cratons, in between mobile belts, and two deep sedimentary basins (Begg et al., 2009). Next to that it is geodynamically influenced by the African Superswell, which is a large topographic anomaly in eastern and southern Africa at an average of 500 m higher than the continental height (Brandt et al., 2011) (Figure 1). Also, the East African Rift System

(EARS), an intracontinental rift zone which supposedly has its terminus in the Okavango Rift Zone (ORZ) in northern Botswana influences its geodynamics (e.g., Fadel et al., 2020; Leseane et al., 2015)(Figure 1). Despite the fact that in recent years different geophysical data has been collected (seismic, gravity, magnetic, magnetotellurics (MT)) (e.g., Fadel, 2018; Gao et al., 2013; Hutchins & Reeves, 1980; Jones et al., 2009), there are still areas and processes that are not well understood. Two major debates are on the supposed location of the terminus of the EARS and the existence and boundary of the buried Maltahohe craton. This paper will provide additional insight into the general tectonic architecture of Botswana and specifically these two debates from the first 3-D inversions of country-wide MT data for Botswana.

The Maltahohe microcraton is an enigma in Botswana geology and geodynamics. There are debates on the actual existence, location, and boundaries of Maltahohe microcraton in southwest Botswana. According to Begg et al. (2009), there may exist an ancient Maltahohe microcraton beneath the Rehoboth Province in southwest Botswana (Figure 1). In an earlier active seismic study, Wright & Hall (1990) interpreted the cratonic structure beneath the Rehoboth Province as a western extension of the Kaapvaal Craton (Figure 1). However, more recent seismological studies in the area argued that the Maltahohe microcraton exist as a separate structure from the Kaapvaal Craton, which is evident from from the observed different Vp/Vs ratios from receiver functions and 3D shear wave velocity models from surface waves (Fadel et al., 2020; Fadel et al., 2018). Similarly, Chisenga et al., (2020), in a study using gravity and aeromagnetic data, supported the existence of the buried Maltahohe microcraton. However, the study argued that the location of the Maltahohe microcraton is likely south of the region suggested by Fadel et al. (2020, 2018). Therefore, it is imperative to study this area further using other data, to confirm or reject the hypothesis on the existence of the Maltahohe microcraton and, if it does exist, understand its boundaries and relationship with the other cratonic blocks.

The extension of the EARS to Botswana is a debated phenomenon in the literature (e.g., Fadel et al., 2020; Khoza et al., 2013; Kinabo et al., 2007; Leseane et al., 2015; Pastier et al., 2017; Y. Yu, Gao, Moidaki, Reed, & Liu, 2015). There are still questions about the existence of rifting in ORZ, and if it exists, its connection with the mature EARS is still debated (Fadel et al., 2020; Khoza et al., 2013; Kinabo et al., 2007; Pastier et al., 2017). Furthermore, there are still varying opinions about the possible further extension of the EARS to central Botswana. The ORZ, which consists of several normal to dextral strike-slip faults is widely interpreted to be the terminus of the western branch of the EARS by several studies (Fadel et al., 2020; Kinabo et al., Modisi, 2008; Modisi, 2000; Modisi et al., 2000; Youqiang Yu, Liu, Moidaki, Reed, & Gao, 2015; Youqiang Yu, Liu, Reed, et al., 2015). However, Pastier et al. (2017) argued that there is no rifting in the Okavango area and proposed a model of differential movement between the Congo and Kalahari Cratons from their geodetic study. Also, from various studies that support the existence of rifting in the ORZ, there are divergent opinions on the rift mechanism and its link to the mature EARS rift. Kinabo et al. (2007), in a gravity and magnetic investigation argued that there is a strong correlation between the orientation of the pre-existing basement fold axes and foliation and the rift induced faults. They inferred that the pre-existing basement structures have significant influence on the development of the rift faults in ORZ. Similarly, Khoza et al. (2013), in a MT study, argued that evidence of continental rifting such as thinned lithosphere and high conductivity mantle anomaly are not present in the ORZ. They proposed a model in which the incipient rifting in ORZ is initiated from the surface and not linked to the EARS. However, Leseane et al. (2015) in a thermal and Moho depth study suggested that the earthquakes in the ORZ are triggered by the migration of fluids from the mantle to the crust. Their results show shallow Curie Point Depths, thin-crust, and high crustal heat from upward movement of mantle fluid to the lithosphere through weak zones beneath the ORZ. Similarly, results from seismic studies, for example Fadel et al., (2020) and Yu, Gao, et al., (2015), showed low-velocity anomaly and mantle seismic anisotropy, which connects to the EARS. These findings provide a piece of evidence for the role of ascending fluids from the EARS in the rifting in ORZ. These various divergent views about the mechanism of the rifting in ORZ and its link with the EARS is yet to be fully understood.

On the further southward extension of the EARS, there was a 6.5 Mw intra-plate earthquake in central Botswana and its possible link to the EARS is still a subject to debate (Figure 1-D) (Gardonio, Jolivet, Calais, & Leclère, 2018; Midzi et al., 2018). The earthquake, which occurred at an approximate depth of 29 km on 03 April 2017 was the second-strongest in magnitude in the country's history and the second strongest intra-plate earthquake in the last 30 years (Gardonio et al., 2018; Midzi et al., 2018). Several studies, including the use of geophysical methods, have discussed the cause of the earthquake. Kolawole et al. (2017), in a combined magnetic, gravity and differential interferometric synthetic aperture radar study, proposed that the 03 April 2017 6.5 Mw earthquake in central Botswana is not linked to the EARS. From their results, the orientation of the tensional stress that caused the earthquake (northeast-southwest) is different from the northwest-southeast directed tensional stress acting on the southwestern end of the EARS. They suggest that the earthquake event was caused by extensional reactivation of a thrust splay in the crust. On the contrary to Kolawole et al. (2017), some studies discussed next suggest the role of fluids or melt the cause of the earthquake (Fadel et al., 2020; Gardonio et al., 2018; Moorkamp et al., 2019). Gardonio et al. (2018) in an interferometric synthetic aperture radar study also suggest that the earthquake event was triggered by stress released from fluid migration from the mantle. Moorkamp et al. (2019) in a study using surface wave and MT data investigated the cause of the earthquake. Their results showed two displaced conductors in the crust which they interpreted to be related to graphite. Their study could neither confirm nor refute the possibility of mantle upwelling fluids as a trigger for the earthquake as suggested by Gardonio et al. (2018). Moorkamp et al. (2019) suggested that passive rifting is a more possible explanation for the cause of the earthquake than thermal weakening from the mantle. Fadel et al., (2020) in a shear wave velocity study argued that the EAR does not only extend to northern Botswana in the ORZ, but that it does extend to central Botswana. From their model, the low-velocity anomaly of the EARS extends to the location of the 03 April 2017 6.5 Mw earthquake in central Botswana. According to Fadel et al. (2020), the process that caused the earthquake suggests that it was associated with fluids or melt from the EARS. These divergent views on the extension of the EARS to Botswana require further exploration and understanding from other geophysical data and models.

In the last two decades, different novel country-wide geophysical data have been compiled and processed in Botswana involving gravity, magnetics, seismic, and MT data. Country-wide gravity and magnetic data provided some of the earliest understanding of the geological provinces and tectonics of Botswana due to the obscuring of the Precambrian geology by thick overburden formed from Kalahari group sediment (Chisenga, et al., 2020; Hutchins & Reeves, 1980; Reeves & Hutchins, 1982; Figure

1-D). Also, several seismological studies have been done to understand the tectonics of Botswana. One of the earliest seismological studies was done by Reeves (1972), which focused on investigating seismicity in the ORZ. Wright and Hall (1990) investigated the Rehoboth Province and its relationship with the Kaapvaal Craton using active deep seismic profiling covering the southwest Botswana. Many years later, several other seismological campaigns covering the eastern and southeast Botswana were done to image high resolution structure of the crust and upper mantle including the temporary network of the Southern Africa Seismic Experiment (SASE) (Carlson et al., 1996) and the Africa Array Initiative (Nyblade et al., 2008). Between 2013 – 2015, the Seismic Arrays for African Rift Initiation (SAFARI) was deployed across the ORZ to further understand the incipient rifting and crustal and upper mantle structure of the region (Gao et al., 2013). More recently, a country-wide seismological project, Network of Autonomously Recording Seismographs (NARS-Botswana) was conducted between 2013-2018 to image the crustal and upper mantle structure beneath Botswana (Fadel, 2018).

Another geophysical data collection in Botswana was the MT data. In 2002, the Southern African Magnetotelluric Experiment (SAMTEX) was started with the aim to image the electrical structure of the crust and upper mantle beneath the southern African region covering Botswana, Namibia, and South Africa (Jones et al., 2009). The MT method gives information about the distribution of electrical conductivity in the crust and upper mantle, which is an independent geophysical information that is not accessible by other methods. Out of the different geophysical properties, electrical conductivity shows the most significant contrasts in the subsurface material with variance spanning up to 14 orders of magnitude, as dry crystalline rocks can have resistivity above 10^6 Ωm, while rocks bearing graphite can have resistivity values below 0.01 Ωm (Simpson & Bahr, 2005; Telford et al., 2004). The wide variance in electrical conductivity gives a potential for producing well-constrained electrical models that can delineate variations in temperature and composition of the Earth's subsurface material.

In the context of our study, the MT method is suitable for imaging different geological terranes and their boundaries using their electrical conductivity properties. Cratonic segments can be delineated from the mobile belts based on conductivity signatures (Muller et al., 2009). Older lithospheric units (Archean Craton) are more resistive than the younger lithospheric units (Proterozoic mobile belts) (Muller et al., 2009). Cratonic boundaries and tectonic transition zones are made of suture zones which are characterized by weakened crust material due to deformation processes (Khoza et al., 2013; Muller et al., 2009). Also, the electrical conductivity model derived from MT data could give a piece of evidence about the presence of aqueous fluids and partial melts, rifting, and rift extensions. While there have been a few studies in Botswana that used the SAMTEX data, the studies so far are focused on regional interpretations or too fragmented and hardly overlap (Evans et al., 2019; Jones et al., 2009; Khoza et al., 2012, 2013; Miensopust et al., 2011; Moorkamp et al., 2019; Muller et al., 2009). This hinders complete imaging and understanding structure of the crustal and upper mantle, and the relationships between the cratons and the mobile belts. Hence, the need to further understand the electrical structure of the crust and upper mantle beneath Botswana.

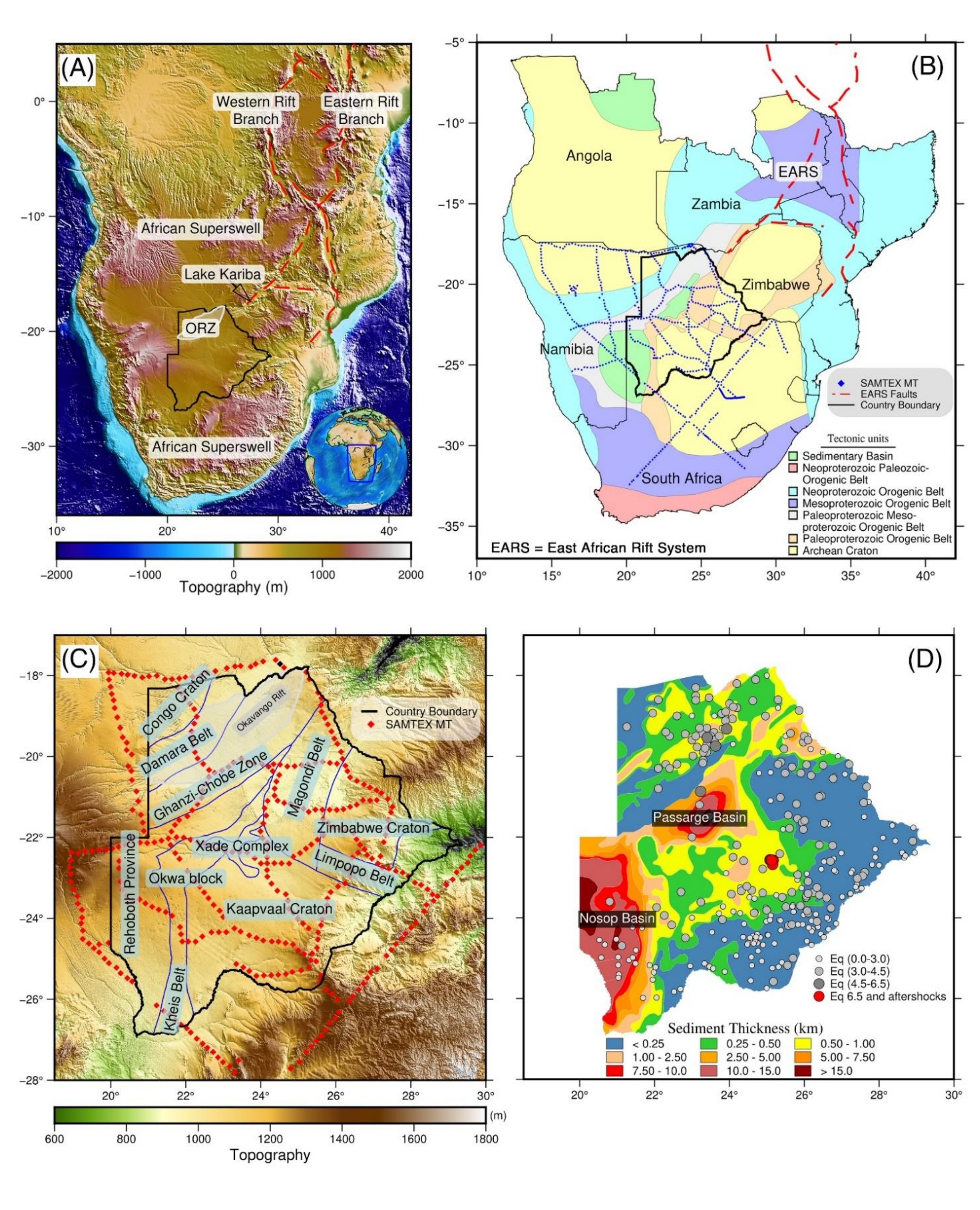

Figure 1: (a) Topographic map of southern Africa, showing the branches of the EARS, the last surface expression of the western branch of EARS at Lake Kariba, the African superswell, Botswana in black outline and the ORZ in white outline. (b) Tectonic map of southern Africa with the distribution of the Southern Africa Magnetotelluric Experiment (SAMTEX) sites (Jones et al., 2009).

(c) Tectonic map of Botswana (McCourt et al., 2013) with the distribution of the SAMTEX data used. The MT station shown in black color represents the ELZ208_94A site and the data from the site are shown in Figure 2. (d) Sedimentary thickness map derived from aeromagnetic data (Pretorius 1984) and earthquake distributions in Botswana with the range of the magnitude represented by 'Eq'.

In this study, we used the MT data to obtain a country-wide three dimensional (3-D) electrical model of Botswana to image the crust and upper mantle besides investigating the Maltahohe microcraton and the extension of the EARS in Botswana. The result of this research provides straightforward, connected, and precise geologic interpretations about the crust and upper mantle of Botswana and arguments raised in the literature about the Maltahohe microcraton and the extension of EARS to Botswana. Our results overcome the fragmented nature of the previous MT studies and the incoherent methodologies and approaches that have led to some conflicting interpretations. The new electrical model of the crust and upper beneath Botswana gives more insight into the tectonic development and the current tectonic settings, cratons deformation, and rift initiation processes in the region.

2. Geology of Botswana

Botswana is located in southern Africa and covers parts of the two cratons in the region and the transitions between them. In Botswana, the Congo Craton covers the northwest region and the Kalahari Craton, which comprises the Zimbabwe and Kaapvaal blocks covers the east and south, respectively (Begg et al., 2009; Figure 1). One of the prominent features in the Kaapvaal Craton is the Bushveld Complex, which is the most extensive layered mafic intrusion into the crust in the world (Begg et al., 2009). The emplacement of the Bushveld Complex in the north-central part of the Kaapvaal Craton (in South-Africa and the far western limb extending to south-east Botswana) took place between 2.06-2.05 Ga (Begg et al., 2009; Haddon, 2005). In southwest Botswana is the Rehoboth Province (Figure), which extends to eastern Namibia. The Rehoboth Province is composed of aggregated mobile belts of Paleoproterozoic age around an Archean nucleus (Van Schijndel et al., 2014; Van Schijndel et al, 2011). There may exist an ancient buried micro craton beneath the Rehoboth Province in Botswana (Begg et al., 2009; Fadel et al., 2020).

In between the cratonic blocks, the lithosphere of Botswana is composed of mobile belts, which were formed from various rifting and accretion processes: Limpopo, Kheis-Okwa-Magondi, Damara, and Ghanzi-Chobe Belts (Begg et al., 2009; Key & Ayres, 2000; Figure 1). The Limpopo Belt is an Archean mobile belt formed from the collision between the Zimbabwe and Kaapvaal Cratons (Begg et al., 2009). The Kheis-Okwa-Magondi Belt composite is a Paleoproterozoic belt covering the central part of Botswana along the western boundaries of Kaapvaal and Zimbabwe Craton (Figure 1). The Damara Belt is a Neoproterozoic Pan-African belt that bounds the southeastern boundary of the Congo Craton (Figure 1). To the southeast of the Damara Belt is the Ghanzi-Chobe Belt (Figure 1), which is composed of sequences of folded meta-sediments (Wright & Hall, 1990). Across the Damara-Ghanzi-Chode Belt is the ORZ, which is considered as an incipient continental rift zone (Kinabo et al., 2008; Modisi et al., 2000; Figure 1).

In central and southwest Botswana, the upper crust includes two sedimentary basins; the Passarge Basin and the Nosop Basin (Figure 1-D). The Passarge Basin is located in central Botswana and is filled with thick and weakly folded siliciclastic and carbonates from the Ghanzi Group sediments with a thickness up to 15 km, and formed during Neoproterozoic and early Paleozoic times (Key & Ayres, 2000; Pretorius, 1984). In the southwest Botswana is the Nosop Basin, which is filled with thick siliciclastic and marine carbonates from of the Nama Group sediments with a thickness up to 15 km during the Neoproterozoic and early Paleozoic times (Begg et al., 2009; Pretorius, 1984; Wright & Hall, 1990).

3. Data and Methods

3.1 Data

We used data from 352 MT sites covering Botswana from the freely available Southern African Magnetotelluric Experiment (SAMTEX) data (Jones et al., 2009; Figure 1-b and 1-c) for the electrical conductivity modelling. The data used consist mainly of broadband MT data from 276 sites and long-period MT data from 76 sites. The robust processing methods described in Jones et al. (1989) was used to process the time series data of the fluctuations of the electric and magnetic field data to MT impedance, apparent resistivities, tipper, and phase data by Jones et al., (2009). Preliminary regional electrical conductivity and electrical anisotropy maps from the SAMTEX data were presented by Jones et al. (2009). Moreover, a recent 3D electrical conductivity model of Southern Africa using the whole SAMTEX data was developed by Ozaydin et al., (2021) and compared with garnet xenocryst from kimberlites for more constrained interpretation of mantle structures. Aside from these regional interpretations of the SAMTEX data, a few other smaller-scale studies have used the SAMTEX data covering small sections within Botswana or across its borders (Evans et al., 2019; Jones et al., 2009; Khoza et al., 2012, 2013; Miensopust et al., 2011; Moorkamp et al., 2019; Muller et al., 2009). For the country-wide 3-D electrical modelling of Botswana, we focused on imaging the electrical structure of crustal and upper mantle in relation to the tectonic development, while providing more insights to some debated hypotheses about its tectonics. We used the full impedance (Z) and tipper data (T) with 31 periods from 0.1 – 10,000 seconds. Incorporating the tipper data into the inversion complements the model development by improving the resolution of the 3-D electrical structures than inversion with standard impedance tensor (Z) only (Becken et al., 2008; Campany et al., 2016). Figure 2 shows an example of the MT data from site ELZ208-94A shown in Figure 1-c.

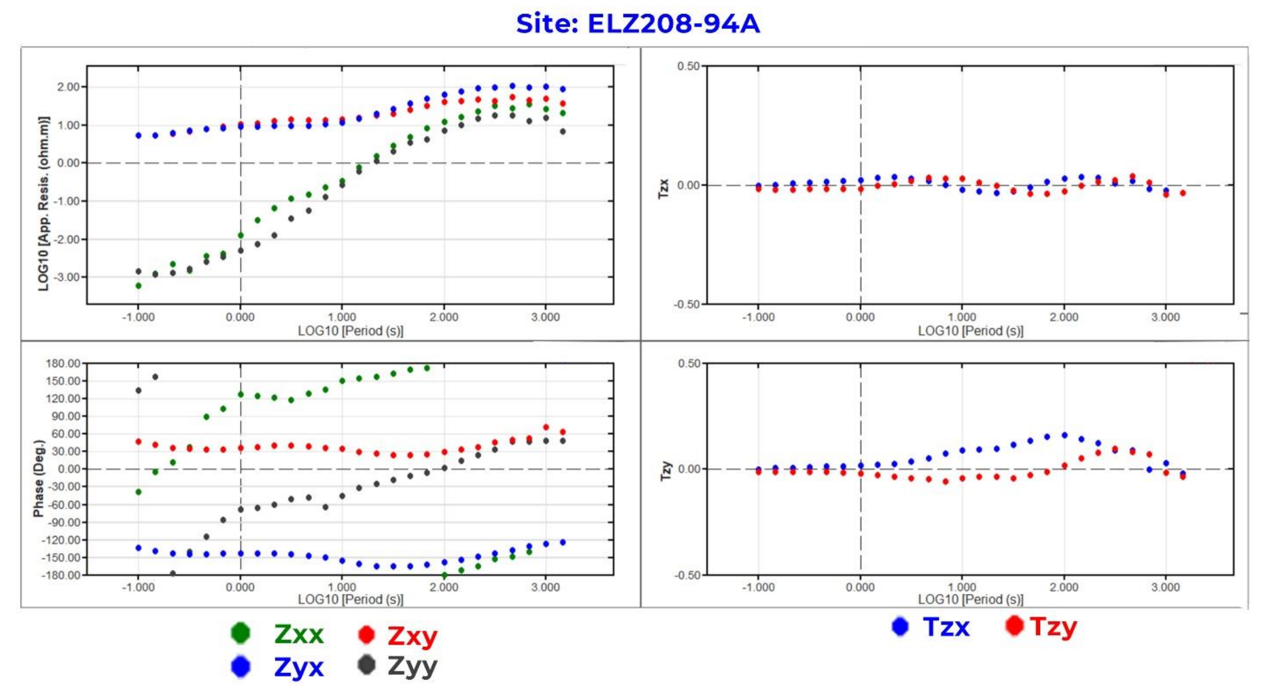

Figure 2: Example of MT data from site ELZ208-94A showing the apparent resistivity and impedance phases against period (in logarithmic scale) for Zxx, Zxy, Zyx, and Zyy components and the tipper components plot against period (in logarithm scale) for Tzx and Tzy.

3.2 Methodology

The methodology we used to derive the 3D electrical conductivity model of Botswana using the nationwide SAMTEX MT data consists of three stages. In the first stage, we processed the MT data for galvanic distortion and error removal to improve the data quality. In the second stage, we analyzed the properties and sensitivity of the MT data by performing depth resolution and dimensionality analysis. Finally, in the third stage, we modelled the MT corrected data using 3-D inversion technique. The details of the methodological steps are discussed further in the following subsections. We used the Python Toolbox for MT data processing, analysis, modelling and visualization (MTpy*;* Kirkby et al., 2019; Krieger & Peacock, 2014). The 3-D inversion of the MT data was done using the Modular System for Electromagnetic Inversion (ModEM) codes (Egbert & Kelbert, 2012; Kelbert et al., 2014).

3.2.1 MT Data Processing

We processed the MT data in two steps. First, we corrected the data for galvanic distortion and static shift error. Subsequently, the distortion corrected MT data were cleaned automatically and visually to remove erroneous data points.

The MT data is often affected by distortions (galvanic distortion) in the electromagnetic field, which are caused by the disturbance of the current that generates the electrical field. Galvanic distortions are non-inductive frequency-independent responses caused by the scattering of regional MT response by accumulated charge distribution on small-scale shallow bodies or inhomogeneity in local geologic structures (Chave & Jones, 2012). Galvanic distortion causes obscuring of the geoelectric strike, phase mixing, masking of properties of regional structures, and distortion of the magnitudes of the impedance tensor. A subclass of the galvanic distortion of the MT data is the static shift, which is a frequency-independent shift in the apparent resistivity curve by a factor (Chave & Jones, 2012; Simpson & Bahr, 2005). In 1-D modelling, static shift causes a shift in the depth to conductive structures and error in the modelled resistivity values. In 2-D and 3-D cases, static shift, if not corrected, may cause artefacts in the model (Simpson & Bahr, 2005). The inherent distortions in the MT data might require corrections to extract undistorted data from the measured data for the purpose of modelling the subsurface electrical structure. According to Chave and Jones (2012) and Meqbel et al. (2014), the scattering effects of small-scale local structures with dimensions or spatial scales larger than the MT site spacing can be modelled in 3-D inversion, and galvanic distortion correction is not required. However, the SAMTEX MT data has high spatial aliasing (Figure 1), hence galvanic distortion removal is necessary. The galvanic distortion removal was done following Bibby et al., (2005) approach, which makes use of phase tensor parameters and implements minimum explicit assumptions about the data parameters. The phase relationship between the magnetic field and electric field remains undistorted and can be used to retrieve the regional impedance tensor (Caldwell et al., 2004). On this basis, Bibby et al., (2005) described an approach of galvanic distortion removal in MT response using the phase tensor, which provides maximum information about the dimensionality of the regional impedance tensor with the minimum assumptions about the data. The phase tensor approach also overcomes the challenges of preconditioned interpretation of regional structures in 2-D along average or dominant strike direction from other techniques (e.g., Groom & Bailey, 1991; Smith, 1995).

Static shift correction factors are generally undeterminable from the MT data itself (Simpson & Bahr, 2005). In this study, we used statistical averaging method to estimate the relative static shift correction factor for each MT station from other stations in the radius of 30 km (Simpson & Bahr, 2005). The outputs of the process are static shift corrected MT responses.

The distortion corrected MT responses were further processed by removing data points with high errors and outliers to improve the convergence of the data in the later inversion process. Poor-quality data points with error bars of the impedance tensor data above 5 percent were removed automatically from the data, which is the error floor used in the later 3D inversion step that will be described later. After that, the MT curve smoothness was done visually on the criteria that the variation in MT apparent resistivity curve from period to period should not be more than 45 ^{o} on a logarithm versus logarithm scale plot. The MT data curves were visually examined and outlying period data points from the MT curve were removed to improve the smoothness of the MT response curve. The distortion corrected and cleaned MT data were subsequently used in the data analyses and modelling stages.

3.2.2 MT Data Analysis

We performed two analyses to determine the sensitivity of the MT data. We performed a depth resolution test to evaluate the depth in the subsurface to which the data is sensitive and can be reliably interpreted. Also, we examined the dimensionality captured in the MT data to understand the most appropriate dimension for modelling the data. To test the depth resolution of the MT dataset, we calculated the depth of penetration of the MT data per station using the Niblett-Bostick transformation (Niblett & Sayn-wittgenstein, 1960). The Niblett-Bostick transformation accounts for variation in depth of penetration for MT sites at similar periods by comparing the MT responses than analysis based only on the period (Adetunji, Ferguson, & Jones, 2015).

The dimensionality of the MT data is an important property which is required to determine the dimension of the modelling approach. The subsurface structure captured in the MT data should have the same dimensionality as the modelling approach used. Modelling MT data in dimensions higher or lower than the dimensionality captured in the data used causes the propagation of the dimensionality distortion in the model, which leads to inaccurate and erroneous interpretation (e.g., a 1-D interpretation of a 2-D or 3-D structure) (Ledo, 2005). We used the phase tensor analysis to examine the dimensionality of the MT data (Booker, 2014; Caldwell et al., 2004). The phase tensor is not affected by galvanic distortion, and it holds essential information about the dimensionality of the MT data (Booker, 2014; Caldwell et al., 2004). The dimensionality analysis showed that the MT data should be modeled in 3D as will be further explained in Subsection 3.1. Therefore, 3D inversion was implemented to invert the distortion corrected and cleaned MT data.

3.2.3 Three-Dimensional MT Data Inversion

We used the ModEM code for the inversion of the MT data (Egbert & Kelbert, 2012; Kelbert et al., 2014). The ModEM utilizes the finite difference approach for forward calculations and the non-linear conjugate gradient (NLCG) technique for solving the inverse problem. The finite difference method is a robust technique for electromagnetic response computation (Egbert & Kelbert, 2012). The NLCG method is generally accepted in the electromagnetics community due to its relative simplicity in solving large inverse problems compared to the other techniques. The NLCG method is efficient because it requires lesser processing units (CPU and memory) as inversion model grids and data increases.

The ModEM 3D inversion code requires constructing starting 3D mesh of the study area with topography and initial electrical conductivity values. Once MT data and starting 3D model are prepared, the inversion process can be executed. Two main parameters govern the inversion process; covariance and initial damping (Kelbert et al., 2014). The covariance (value between 0 – 1) controls how the norm of the model behaves. Large covariance values result in smoother models with poor data fit, while small covariance values result in rough models with higher data fit (Robertson, Thiel, & Meqbel, 2020). On the other hand, the initial damping parameter controls how the model fits the data progressively.

The distortion corrected and cleaned MT over Botswana was inverted using a 3D mesh with a cell dimension of 10 km × 10 km in the horizontal plane. The choice of the horizontal griding dimensions was based on the minimum interstation spacing in the data. A first layer thickness of 50 m was used, and the subsequent vertical layers' thicknesses increased by a factor of 1.1 logarithmically. The mesh is composed of 137, 138, and 100 cells in the X, Y, and Z directions. A resistivity value of 100 Ωm was used for the starting model (Robertson et al., 2020). Also, an error floor ($\sqrt{|Z_{xy}Z_{yx}|}$) of 5% was used for the Z_{xy} and Z_{yx} impedance data, an ($\sqrt{|Z_{xx}Z_{yy}|}$) of 5% was used for the Z_{xx} and Z_{yy} impedance data, and an 0.03 error floor for the tipper data (Meqbel et al., 2014). Topography data was incorporated into the model to compensate for site elevation difference in the data. Ten air layers were added to the starting model to pad the Earth model. A covariance value of 0.4 was used to resolve less smooth features and create a geologically plausible electrical model (Robertson et al., 2020). ModEM initial damping parameter of 10 was used for the inversion to minimize required computation time and resources (Robertson et al., 2020). The final misfit for the electrical conductivity model is 3.22 after 148 iterations. Details of the model misfit is discussed in section 3 of the SM and Figures S11 – Figure S14 in the supporting material (SM).

We carried out several inversions to investigate the sensitivity of the inverted electrical model to three main parameters; the grid resolution, the initial damping parameter, and the possibility of the retrieved low conductive anomalies with values between 1-10 Ωm in the inversion results. A covariance value of 0.4 was fixed for all tests, similar to main inversion covering Botswana described before (Robertson et al., 2020). For the sensitivity tests, smaller datasets were used to ensure that the computational time required is shorter. Details about the sensitivity tests are discussed in the supplementary material (SM). In the following, we briefly describe three sensitivity tests on the initial damping parameter, model grid resolution, and high conductivity structures.

(1) We investigated how the initial damping parameter affects the resultant electrical model with varying values of 1, 10, 100, and 1,000.
(2) Model grid resolution determination is an important step in 3-D MT inversion. The decision of the size of the model grid is usually balanced between the need to recover fine model details by using a higher-resolution grid and, on the other side, minimizing the computational time and resources required by using a coarser-resolution grid. We investigated how the horizontal grid resolution affects the resultant electrical model using a coarse grid of 30 km × 30 km, an intermediate grid of 15 km × 15 km and a fine 10 km × 10 km grid resolutions.
(3) A major uncertainty in our electrical modelling result was the highly conductive structures (1–10 Ωm) in the lower crust and upper mantle depths. A sensitivity test was carried out to verify the certainty of these high conductivity structures if they are data related. The test involved removing the conductive structures in the model and replacing them with the resistivity of the starting model (100 Ωm). The inversion is then restarted with the modified model. The resultant model was examined to see whether the high conductivity structures are returned in the model or not.

4. Results and Discussion

4.1 Resolution Depth and Dimensionality

The results of the resolution depth and the dimensionality of the MT data are presented and discussed in detail in the SM (Figure S1 – S5). Here, we discuss the main findings. The conclusion from the depth resolution test is that the MT data used in this study can image down to 200 – 250 km depth (Figure S1). The electrical models are presented up to depth of 200 km and sensitivity depth per MT site are also indicated (Figure 4-6). The MT data is not only sensitive to depths but also to the volumetric electrical conductivity of the subsurface as electromagnetic waves have a diffusive nature. The lateral distance to which the MT data is sensitive at any depth is referred to as horizontal adjustment length. At the various depth of penetration of the MT data, the horizontal adjustment length is approximately 2 – 3 times the value of the penetration depth (Simpson & Bahr, 2005). However, due to high spatial aliasing between the MT sites (Figure 1), at shallow depths, the horizontal adjustment lengths are small. Hence, the results of the electrical model are interpreted and discussed along cross-sections on top or in the near proximity of the MT stations (Figure 3 - Figure 5) to address the shortcoming of the small horizontal adjustment length.

The results of the dimensionality analysis (Figure S2 – Figure S5 in SM) show high skew values (up to 6º) and high ellipticity of the phase tensor for majority of the MT sites. High skew values of the phase tensor greater than 6º indicate 3-D effects, skew values of 0º indicate 2-D data, and lower skew values indicate 1-D subsurface structure (Cherevatova et al., 2015; Comeau et al., 2020). When the phase tensor is a circle, it indicates 1-D subsurface, while the elliptical phase tensor represents 2-D or 3-D effects in the conductivity distribution (Becken & Burkhardt, 2004; Bibby et al., 2005). Hence, the results indicate the presence of 3-D signature in the MT dataset.

The previous MT studies done in Botswana using the SAMTEX data (e.g., Miensopust et al., (2011), Muller et al., (2009), and Khoza et al., (2012)) confirmed the presence of 3-D signature in the MT data. There exist multiple principal geoelectric strike directions in the MT data, which is indicative of 3-D structure (e.g., Miensopust et al., (2011), Muller et al., (2009), and Khoza et al., (2012)). The result of the phase tensor analysis confirms the 3-D nature of the structure beneath Botswana as reflected in the MT data. Therefore, the MT data for this study were modelled in 3-D without need for assumption of geoelectric strike directions, which is required for 2-D modelling approach.

4.2 Sensitivity Tests

The results of the sensitivity tests are presented and discussed in the SM. Here we highlight the main findings on the inversion initial damping parameter, grid resolution, and conductive structures.

4.2.1 Initial Damping Parameter

The different initial damping parameter tested (1, 10, 100, and 1,000) did not influence the data fit nor the resolved structures in the resultant models (Figure S6 in SM). However, higher initial damping parameters took longer NLCG iterations and computation time to achieve convergence of the inversions. These observations are consistent with the results from model space exploration with the Australian Lithospheric Architecture Magnetotelluric Project data using the ModEM codes done by Robertson et al. (2020). For the inversions in this study, we used an initial damping parameter of 10 to reduce the computing time (Robertson et al. 2020).

4.2.2 Grid Resolution

We observed that increasing the grid resolution from 30 km to 15 km and from 15 km to 10 km led to increase in the data fit of the resultant model (Figure S7 in SM) and geologically plausible electrical structures (Figure S8 and Figure S9 in SM). A choice of 10 km horizontal grid resolution, which is also the minimum interstation spacing in the data was made to recover a high-resolution model that can better fit the MT data.

4.2.3 Conductive Structures

We observed that the high conductivity structures with resistivity values between 1 – 10 Ωm in the crust and upper mantle in our electrical model are required and are data related. From the test, the highly conductive features return to the model after a continued inversion of the modified model as described in section 2.2.3 (Figure S10).

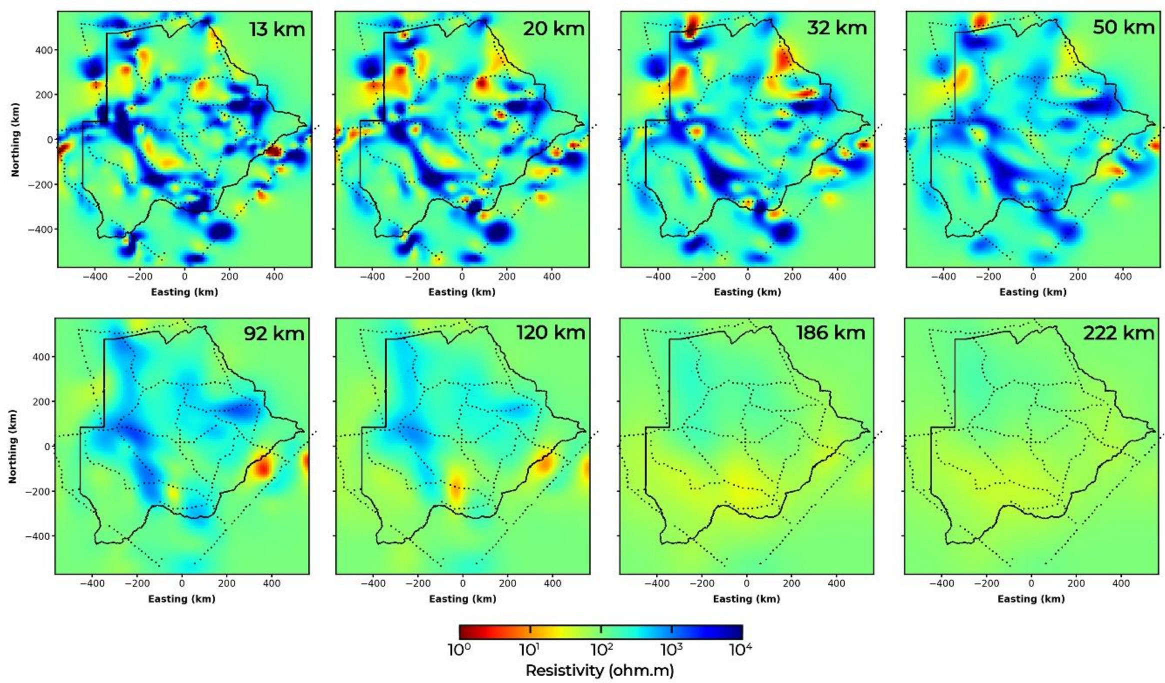

Figure 3: Plan view of electrical conductivity model depth slices at 13 km, 20 km, 32 km, 50 km, 92 km, 120 km, 186 km, and 222 km depths. MT sites are represented in black dots.

4.3 The Electrical Conductivity Model

The final 3-D electrical model of Botswana is presented as depth slices in Figure 3 and cross sections in Figure 4 to show the variation of the electrical conductivity of the different tectonic terranes in the study area. The cross sections were chosen along the data profiles to overcome the shortcoming of small horizontal adjustment length at shallow depth and make the results reliably interpretable.

From the results (Figure 3 and 4), there are distinctive high conductive structures, both in the crust and upper mantle in the region. Several factors can contribute to the high conductivity in the mid-lower crust and upper mantle. Anomalous conductive structures in the lower crust can be interpreted as the presence of graphite or aqueous fluids (Jones et al., 2005). In some areas, sulfides and other metalliferous ore deposits or partial melt contribute to high conductivity in the lower crust (Wannamaker et al., 2008). The areas that are spatially close to suture zones or fault zones also have high conductivity features due to the weakening of the crust (Jones, Ledo, & Ferguson, 2005). In the mantle, high conductivity anomalies can be due to high temperatures, partial melting, hydration, or mineralization of the mantle material (such as iron enrichment) from magmatic intrusion (Evans et al., 2019; Jones et al., 2005; Khoza et al., 2012, 2013).

In southwest Botswana (Figure 4; A-A'), there are distinctive electrical structures across the Rehoboth Province, Kheis Belt, and the Kaapvaal Craton. The Kheis Belt has the lowest bulk electrical resistivity, while the Kaapvaal Craton has the highest bulk electrical resistivity. The Kaapvaal craton is imaged as a highly resistive structure (approximately 10,000 Ωm). The Kheis Belt is imaged next to the Kaapvaal Craton as a relatively less resistive lithosphere (500 – 1,000 Ωm). Beneath the Rehoboth Province, the result shows a separate resistive structure (with average resistivity above 1,000 Ωm) between 30 km to 100 km depth. This signature is indicative of a cratonic structure. However, there is broad conductive structure from the upper mantle (100 km) downward across the profile A-A', which could be due to high temperatures regimes in the mantle (Sobh, et al., 2021). The observed lateral variation across the Rehoboth Province-Kheis Belt-Kaapvaal Craton is confirmed by the shear wave velocity model by (Fadel et al., 2020).

Figure 4 (B-B') shows distinctive electrical structures across the Okwa Block and the Kaapvaal Craton. The Okwa Block is imaged as a resistive structure (~ 1,000 – 10,000 Ωm) with the presence of a conductor (~ 10 Ωm) at a depth of ~40 km. The Kaapvaal Craton is imaged as a resistive structure. However, from the depth of ~100 km downward, there exist a broad highly conductive structure (~5 Ωm), which may be due to iron enrichment of the mantle from the emplacement of the Bushveld Complex. In the northwest margin of Botswana (Figure 4, C-C'), the Congo Craton is imaged as a resistive structure. In the Damara-Ghanzi Chobe Belt (C-C'), there are distinctive highly conductive structures in the crust (~30 km) and at a deeper depth (~80 km downwards) around the east of profile C-C'. The highly conductive structures along the C-C' profile may be due to fluids or melts from the EARS. Cross section D-D' shows the electrical conductivity model across Congo Craton, Damara-Ghanzi Chobe Belt (ORZ) and the Magondi Belt. The Congo Craton is imaged in northwest Botswana as a highly resistive structure with the presence of a crustal conductor which may be due to presence of ironstone in the metasedimentary rocks of Xaudum Group (Begg et al., 2009; Chisenga, Jianguo, et al., 2020). In the Damara-Ghanzi-Chobe Belt, the ORZ is imaged as a highly conductive crustal structure (~5 Ωm) that connects with mantle structure of intermediate conductivity (Figure 4, D-D'). Similarly, in Magondi Belt, a highly conductive crustal structure (~1 Ωm) is imaged, which seems to connect with a conductive mantle structure. These structures can be interpreted to be due to the upward movement of fluids or melt from the mantle to the crust beneath the ORZ and the Magondi Belt through zones of weakness as suggested by previous studies (e.g., Fadel et al., 2020).

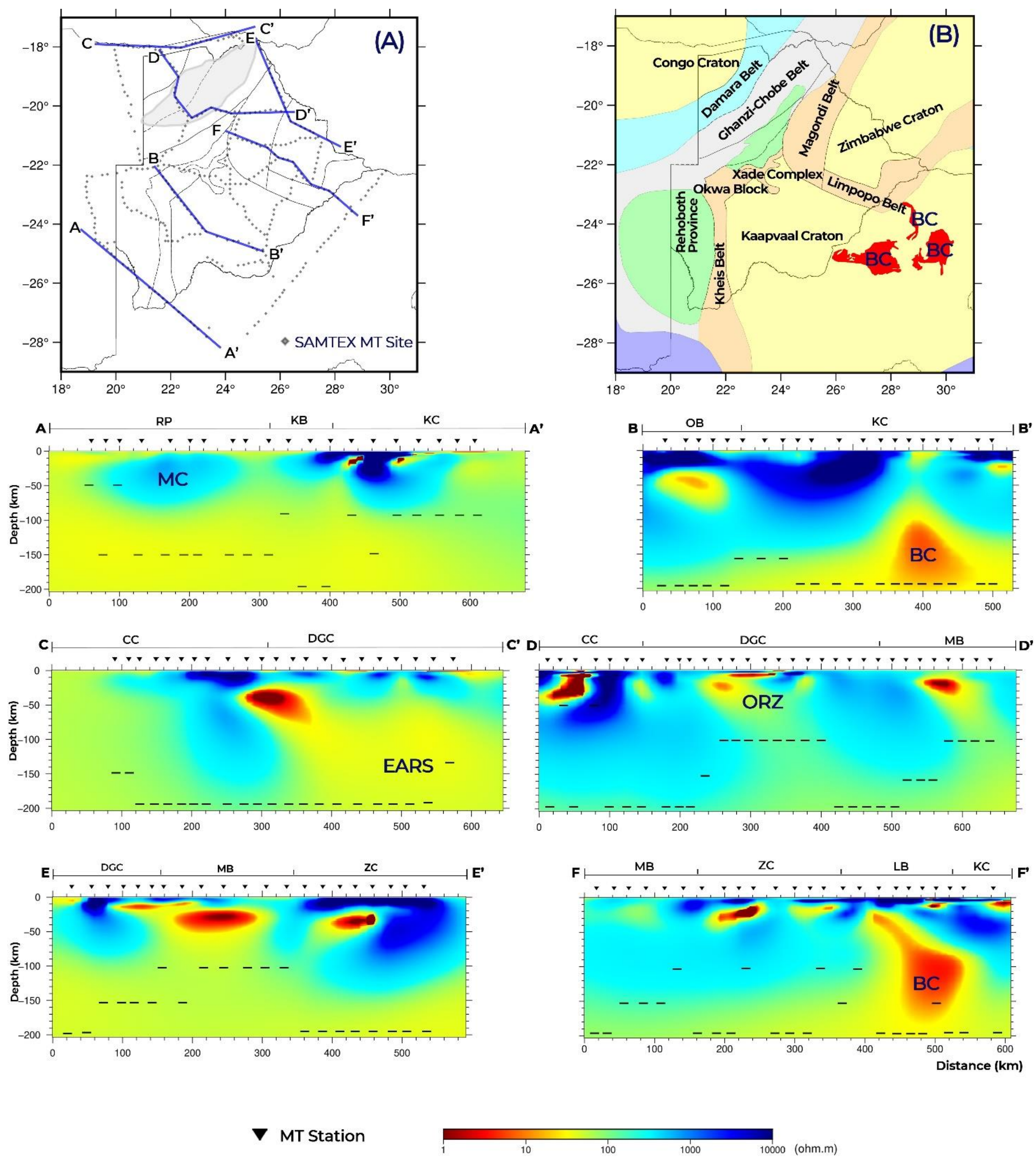

Figure 4: The 3-D electrical conductivity model of Botswana along 5 cross sections represented with blue lines in (a). RP = Rehoboth Province; KB = Kheis Belt; KC = Kaapvaal Craton; OB = Okwa Block; CC = Congo Craton; DGC = Damara-Ghanzi-Chobe Belt; MB = Maagondi Belt; ZC = Zimbabwe Craton; LB = Limpopo Belt; MC = Maltahohe microcraton; ORZ = Okavango Rift Zone; EARS = East African Rift System; BC = Bushveld Complex. Black dashes underneath each MT station in the electrical model = depth sensitivity per MT site.

Figure 4; F-F’ shows the electrical conductivity model across the Magondi Belt, Zimbabwe Craton and the Limpopo Belt. The Zimbabwe Craton is imaged as a highly resistive structure with the presence of crustal conductive structures which may be due to presence of graphite and/or sulfide (Khoza et al., 2012). The observed high resistivity structure of the Zimbabwe Craton is consistent with results from seismic models. There is a region of high-velocity anomalies beneath the Zimbabwe Craton (Fadel et al., 2020; Ortiz et al., 2019; White-Gaynor et al., 2021). Another feature of note along F-F’ is the highly conductive structure, which may be due to iron enrichment during the Bushveld Complex beneath the Kaapvaal Craton and the Limpopo Belt. This observation is consistent with a region of low velocity beneath the Limpopo belt from seismic studies (Ortiz et al., 2019). They support that this region of low velocity resulted from modification of the lithospheric and the mantle material by the Bushveld Complex magmatic event.   of the Magondi Belt is imaged as a conductive structure (Figure; E-E’). Miensopust et al. (2011), in a previous MT study in northeast Botswana, observed crustal conductors beneath the Magondi Belt and suggested the structures to be most likely due to the presence of graphite or sulphide. The Magondi belt was accreted to the Kheis-Okwa Belt (Thomas, von Veh, & McCourt, 1993), and the Kheis-Okwa-Magondi Belt composite was modified during the Bushveld Complex emplacement (Begg et al., 2009).

4.4 Velocity-Conductivity Interpretation

Seismology and magnetotelluric methods are two primary geophysical methods for studying the structure of the crust and upper mantle because of their capacities to image deep Earth structures (Panza et al., 2006). These two methods look at different independent physical properties; velocity and conductivity, and they have different sensitivities to subsurface structures. Therefore, there is usually no complete match between the seismic velocity models and the electrical models. However, using both methods may support and complement some interpretations of subsurface structures. Here, we complement the interpretations from our new 3-D electrical conductivity model with the country-wide 3-D shear wave velocity model of Botswana by Fadel et al. (2020) to arrive at better interpretations (Figure 6). Their results included investigation of similar tectonic domains of this paper; the Maltahohe microcraton and the extension of the EARS to Botswana, which are discussed in detail in coming sections (Figure 6).

4.5 The Maltahohe Microcraton

The resistive structure beneath the Rehoboth Province (Figure 4, A-A’) indicates the presence of a cratonic structure from depths of 10 km to 100 km. This cratonic structure is clearly separated from the Kaapvaal Craton, with the Kheis Belt imaged in between both. We interpret the cratonic structure beneath the Rehoboth Province as the Maltahohe microcraton being separated from the Kaapvaal Craton. This is contrary to the proposition of thinned western extension of the Kaapvaal Craton by Wright and Hall (1990). In an earlier MT study, Muller et al. (2009) carried out a 2-D interpretation of the MT data across Kaapvaal Craton, Rehoboth Province and Damara-Ghanzi-Chobe Belt. According to the data decomposition study by Muller et al. (2009), multiple geoelectric strike directions are present in the data, which could be best solved using 3-D modelling approach. However, they inverted the MT data independently in two geoelectric strike directions of 25^{o} and 45^{o} due to computational limitations. Their electrical model showed conductive and resistive blobs beneath the Rehoboth

Province, which could be due to dimensionality distortion in their 2-D interpretations. With recent advancements in high performance computing, 3-D modelling are possible. The improved 3-D modelling methodological approach we employed helped to improve the imaging of the cratonic structure beneath Rehoboth Province, which we interpret as the Maltahohe microcraton. The 3-D MT modelling does not require assumption on geoelectric strike direction, which prevents dimensionality distortion in the interpretation of the electrical model compared to the previous 2-D modelling.

The finding from our 3-D electrical model on the existence of the Maltahohe microcraton is consistent with some previous studies (e.g., Begg et al., 2009; Chisenga, Jianguo, et al., 2020; Fadel et al., 2020). Our finding also confirms the location of the Maltahohe microcraton to be similar to Fadel et al. (2020) and that is it a separate cratonic structure from the Kaapvaal Craton (Figure 4, A-A' and Figure 6; II-II'). Fadel et al. (2020), from their 3-D shear wave velocity study, observed a positive shear wave velocity beneath the Rehoboth Province interpreted as the Maltahohe microcraton. In the shear wave velocity model, the high velocity structure of the Maltahohe microcraton is imaged up to 200 km depth as compared to 100 km depth in the electrical model (Figure 6; I-I' and II-II'). The disparity in the imaged depth may be due to low MT site coverage along the II-II' profile. In the unresolved section along the II-II' profile (low MT site coverage), the conductivity model could not image the possible deeper sections of the Maltahohe microcraton compared to the 3-D shear wave velocity model.

4.6 The Bushveld Complex

Fouch et al. (2004), in a seismic study, observed low seismic wave velocities in the Bushveld Complex around the southeastern border of Botswana. The location of the low seismic anomaly from the model of Fouch et al. (2004) coincides with the interpreted Bushveld Complex high conductivity anomaly along B-B' in Figure 4. Fouch et al. (2004) suggested that the low seismic wave velocity anomaly linked it to compositional changes in the mantle due to iron enrichment from the formation of the Bushveld Complex. Similarly, other seismic investigations, including the P and S wave velocity study by Ortiz et al. (2019) and the shear-wave velocity study by White-Gaynor et al. (2021), shows a region of low velocities beneath the Bushveld Complex in the Kaapvaal Craton. Ortiz et al. (2019), supporting Fouch et al. (2004), argued that the low velocities anomalies observed beneath the Okwa Block, Magondi Belt and Limpopo Belt, which are extensions of the Bushveld Complex, are results of the modification of the composition of the mantle material from the magmatic event. Ortiz et al. (2019) ruled out the possibilities of thermal anomalies as the cause of these low-velocity anomalies since no tectonic event affected these terranes in the Phanerozoic age.

In a previous MT study across the Kaapvaal Craton, Evans et al. (2011) found high electrical conductivity structure of ~10 Ωm in the Bushveld Complex. The interpreted MT data profile by Evans et al. (2011) intersects with the interpreted Bushveld Complex high conductivity anomaly in cross section F-F' in Figure 4. From their MT study, Evans et al. (2011) suggest that connected metallic sulphides, iron-rich garnets, and other economic minerals form the network of conductors within the Bushveld Complex. This is similar to the proposition of Jones and Garcia (2006) for the high conductivity anomalies beneath the Yellowknife River Fault zone in the Slave Craton in northern Canada. From the result of our model, there is an anomalous highly conductive structure from ~100 km downwards beneath the Kaapvaal Craton (Figure 4, B-B' and F-F'). Jones (1988) reported that the geotherms in the Bushveld Complex are insignificantly higher compared to other parts of the Kaapvaal Craton from heat flow data. Also, the last thermal event in the emplacement of the Bushveld Complex occurred in the Archean (Begg et al., 2009; Evans et al., 2011). With these pieces of evidence, this study, supporting the interpretation of Fouch et al. (2004), attributes the iron enrichment of the mantle material from the Bushveld Complex emplacement as the cause of high conductivity structure (Figure 4; B-B').

4.7 The Extension of the East African Rift System to Botswana

The southwestern branch of the EARS is often interpreted to have its terminus in northern Botswana (e.g., Fadel et al., 2020; Leseane et al., 2015; Modisi, 2000; Ortiz et al., 2019; Youqiang Yu, Gao, et al., 2015). The southernmost surface expression of the EARS occurs at Lake Kariba, near the northeastern tip of Botswana (Figure 1). Our study investigates the possible extension of the EARS in Botswana. The electrical conductivity model across the northern border of Botswana in Namibia along the MT sites shows a distinctive high conductivity anomaly in the lower crust (~30 km), which connects with a conductive structure in the mantle (~80 km downwards; Figure 4 C-C'). This highly conductive mantle structure may be due to the further subsurface extension of the EARS from lake Kariba. The high conductive anomaly in the lower crust (Figure 4, C-C') could be due to the migration of fluids or melt from the EAR into the crust through zones of weakness. In the ORZ, we found a highly conductive crustal structure (~5 Ωm) that connects with a conductive upper mantle structure, which also supports the interpretation of ascending fluids or melt as the cause of the rifting in the ORZ (Figure 4, D-D'). This mechanism of ascending fluids or melt from the mantle to the crust is similar to the interpretation by Fadel et al., (2020) from cross sections across the ORZ in northern Botswana from their shear wave velocity model. Their velocity model shows that the mantle low-velocity anomaly, which is linked to the EARS seems to connect with the shallow low-velocity anomaly of the ORZ (Figure 6; J-J') (Fadel et al., 2020). Both cross sections C-C' and D-D' from the electrical model are spatially displaced from the cross-section J-J' from the shear wave velocity model. However, the mechanism of ascending fluids or melt from the mantle to the crust is similar to the proposition of Fadel et al. (2020) about the rifting in the ORZ. The interpretation of the conductive anomaly beneath the ORZ in our electrical model is supported by a high Vp/Vs ratio from the by receiver function studies (Fadel et al., 2018; Yu, et al., 2015) and shallow Curie depth from aeromagnetic data (Leseane et al., 2015). According to Leseane et al. (2015) and references therein, it is suggested that the earthquakes in the ORZ are triggered by the migration of fluids from the mantle to the crust. Our interpretation also support the proposition by Fadel et al., (2020) on the role ascending fluids from the EARS in the weakening of the lithosphere and subsequent rifting in the ORZ. However, there exist contrary opinions on the extension of the EARS to northern Botswana and mechanism of the incipient rifting in the ORZ (e.g., Khoza et al., 2013; Kinabo et al., 2007; and references therein). Khoza et al. (2013), in a previous MT study covering parts of northwest Botswana, argued that neither a thinned lithospheric structure nor high conductivity mantle anomalies are present beneath the ORZ from their electrical model. They go further to propose a model in which the incipient rifting in ORZ is initiated from the surface. The result from our 3-D electrical conductivity model provides a piece of evidence for the ascending fluids from the EARS to the crust in the northern border of Botswana with Namibia in a similar mechanism as suggested for the ORZ by Fadel et al., (2020).

Furthermore, Fadel et al., (2020) suggested that the EARS does not only extend to the ORZ, but further extends to central Botswana from their velocity model. Cross-section K-K' (Figure 6) in the shear wave velocity model shows a connection between a low-velocity anomaly beneath the epicentre of the 03 April 2017 6.5 Mw earthquake and a deeper low-velocity anomaly that may be due to the EARS. According to Fadel et al. (2020), the ascending fluids or melt from the EARS into the region below central Botswana may be the cause of the 6.5 Mw earthquake. Similarly, Chisenga et al. (2020) modelled the crustal thickness of the crust beneath Botswana using gravity data. From their results, the crust beneath the epicentre of the 03 April earthquake in central Botswana is relatively thinner with an approximate thickness of 40 km compared to 43 km and 46 km thicknesses in the adjacent Kaapvaal Craton and central part of Limpopo Belt, respectively. Their result suggested that the thinning of the crust beneath the earthquake epicentre was caused by migrating thermal fluids from the EARS, eroding the lower crust structure. They propose that the combination of migrating thermal fluids from EARS, high heat flow, thin-crust and local stress in the crust contributed to the 03 April earthquake occurrence.

Our electrical conductivity model is not able to confirm or refute the proposition of EARS' extension to central Botswana because of under sampling of the MT data along the transect to investigate the phenomenon (Figure 5; G-G'). Hence, the electrical conductivity model is not able to provide more insight into the extension of the EARS to central Botswana. At shallow depth of penetration of the MT data, the horizontal adjustment length to which the data is sensitive is small, and the structures recovered are more local. Due to this, shallow structures that are laterally far away from the MT sites cannot be reliably interpreted along the G-G' transect. At large depths, approximately greater than 100 km, the horizontal adjustment length increases and the MT response at the MT site becomes more regional. Hence, the structures in the model that are laterally displaced from the MT sites can also be reliably interpreted. At the epicenter of the 03 April 2017 6.5 Mw earthquake, the model shows a high conductivity anomaly at a depth of 30 km, which is resolved by at least one MT site. Moorkamp et al. (2019) in a study in central Botswana using surface wave and MT data found two displaced conductive structures which were interpreted as likely related to graphite. Their MT and seismic velocity results suggest the reactivation of the old fault zone associated with a weak mantle because of amphibole enrichment and reduced grain size. While they did not confirm or refute the concept of mantle upwelling fluids as a trigger for the earthquake, they attributed the earthquake and the associated weak mantle below to a more likely passive rifting related to the ambient stress field driven from top to bottom rather than thermal weakening from below. Also, Moorkamp et al. (2019) suggest that the earthquake reactivated existing fault from the deformation process of the collision between Kaapvaal and Zimbabwe cratonic blocks. However, Fadel et al., (2020) and Chisenga et al. (2020) suggest that ascending fluids or melt is linked to the EARS deep feature at northern Botswana that extends through the weak lithospheric zones in the region and played a role in triggering the earthquake.

There is also a high conductivity anomaly in the northern part of this cross-section from the depth of about 100 km, which is resolved by at least two MT sites at such depth. We interpreted this high conductivity structure as the possible extension of the EARS to northern Botswana. Another feature of note is the conductive structure beneath the Kaapvaal Craton from a depth of 120 km, which is resolved by at least three MT sites at that depth. This high conductivity structure may be due high temperatures regimes in the upper mantle or from iron enrichment from the Bushveld magmatic emplacement in the

Kaapvaal Craton. Additional MT measurements along this transect are required to resolve the electrical structure of the crust and upper mantle and further investigate the suggested extension of the EARS to central Botswana and its role in the 03 April 2017 6.5 Mw earthquake in central Botswana.

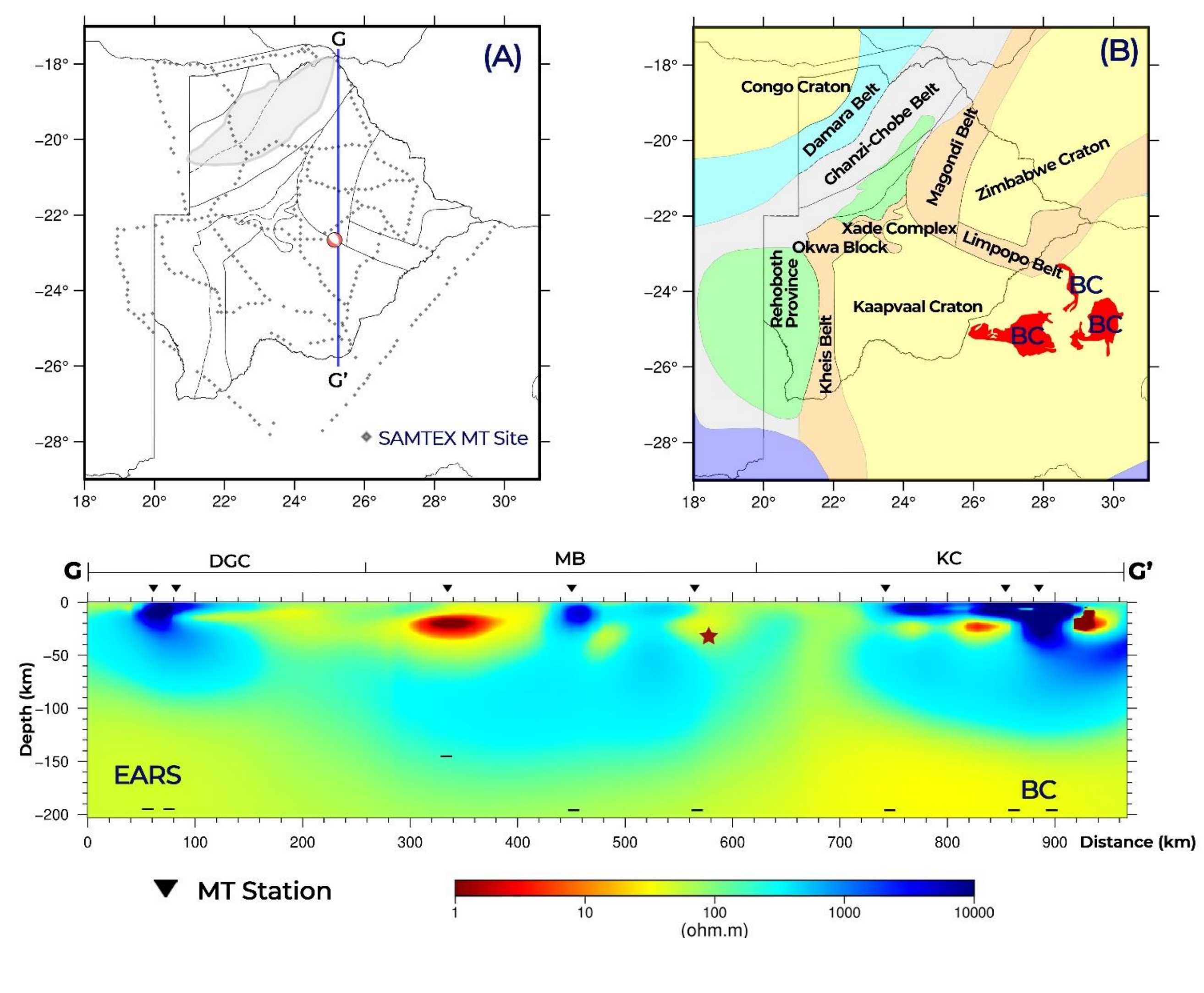

Figure 5: Electrical conductivity model north-south cross section (represented with blue line in (a)) across the epicenter of the 03 April 2017 earthquake in central Botswana. DGC = Damara-Ghanzi-Chobe Belt; MB = Magondi Belt; KC = Kaapvaal Craton; EARS = East African Rift System; BC = Bushveld Complex. Black dashes underneath each MT station in the electrical model = depth sensitivity per MT site.

5. Summary and Conclusions

We presented the 3-D electrical conductivity model of Botswana derived from MT data. Our homogenous 3-D modelling approach for interpreting the MT data covering Botswana overcame the preconditioned 2-D interpretation of the electrical structure of the crust and upper mantle along average geoelectric strike directions. Besides this, the country-wide electrical modelling provides a connected and precise interpretation of the electrical structure, overcoming the limitations of fragmented nature of the previous MT studies in Botswana. Our electrical model showed significant structures in the crust and upper mantle of Botswana. The model highlights the main geologic terranes in Botswana, including the very resistive structures of the cratonic terranes - Congo, Kaapvaal, Zimbabwe Cratons and Rehoboth Province; and the less resistive structures of the mobile belts - Damara-Ghanz-Chobe, Limpopo, and Kheis-Okwa-Magondi Belts. In southwest Botswana, we find a distinctive resistive structure beneath the Rehoboth Province, which suggests the existence of the Maltahohe microcraton as a separate cratonic unit as proposed by other studies. In addition to these, we imaged a highly conductive anomaly in the crust beneath the ORZ, which connects to a deeper high conductivity anomaly that may be related to the last surface expression of the EARS. We suggest that ascending fluids or melt from the EARS, which causes the weakening of the lithosphere, play a significant role in the incipient continental rifting in the ORZ. Lastly, our electrical model is not able to confirm or refute the suggested extension of the EARS to central Botswana. Additional MT data measurements along northeast to central Botswana would solve the challenge of under sampling and help resolve the electrical structure in this transect better.

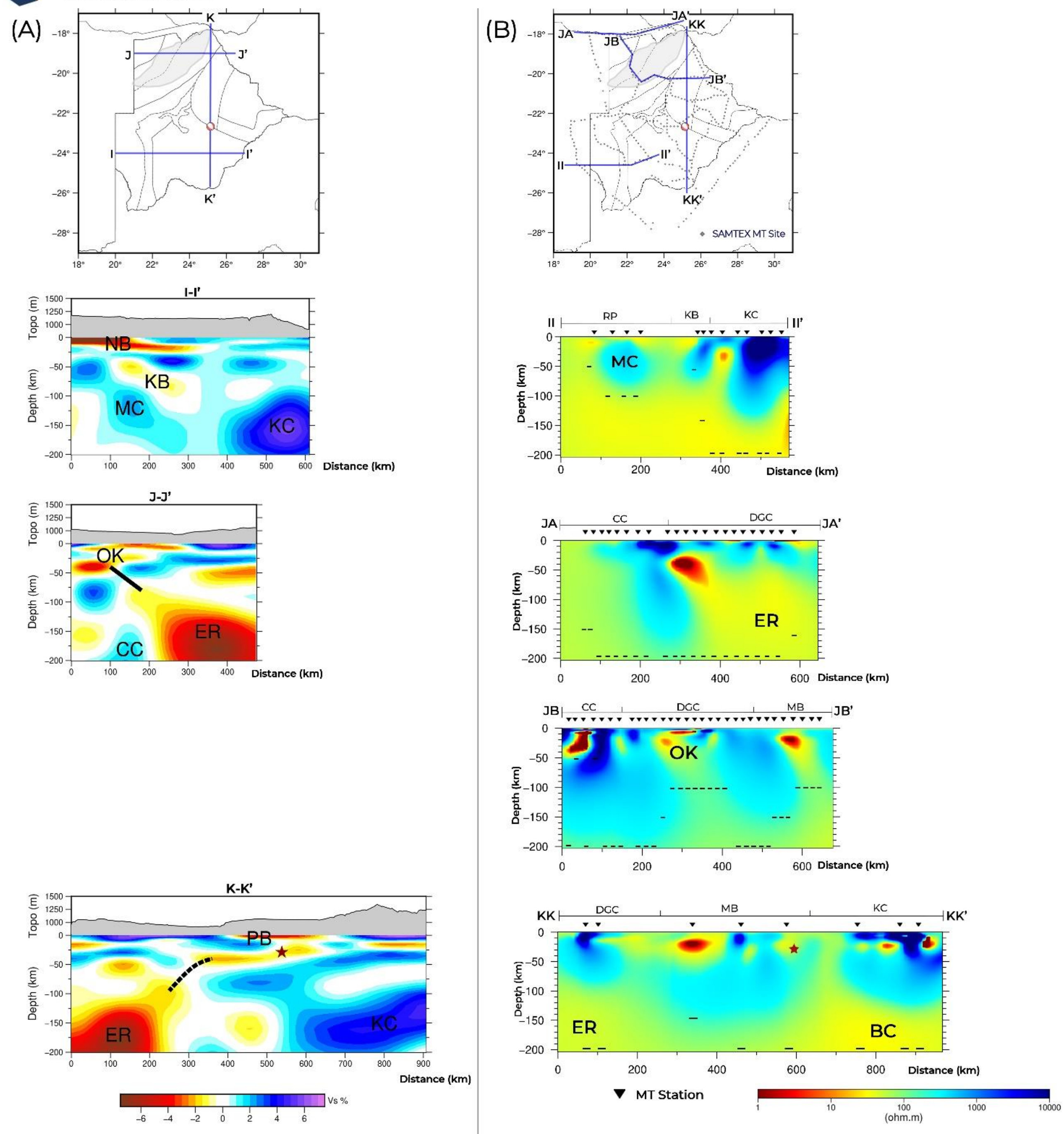

Figure 6: (a) The 3-D shear wave velocity model of Botswana after Fadel et al. (2020). (b) Electrical conductivity model derived from MT data. The red star = location of the 6.5 Mw earthquake in 2017. The highlighted features are; CC = Congo Craton, DGC = Damara-Ghanzi-Chobe Belt, ER = East African Rift System, KC = Kaapvaal Craton, KB = Kheis Belt, MB = Magondi Belt, MC = Maltahohe microcraton, NB = Nosop Basin, OK = Okavango Rift Zone, PB = Passarge Basin, and RP = Rehoboth Province; BC = Bushveld Complex. Black dashes underneath each MT station in the electrical model = depth sensitivity per MT site.

Acknowledgement

The freely available SAMTEX data was used in this study (https://www.mtnet.info/data/samtex/samtex.html). The SAMTEX was conducted to image the electrical structure of the crust and upper mantle beneath the southern African region, covering Botswana, Namibia, and South Africa (Jones et al., 2009) (Figure 1). The authors wish to acknowledge the contributions of the SAMTEX consortium comprising: The Dublin Institute for Advanced Studies, Woods Hole Oceanographic Institution, the Council for Geoscience, De Beers Group Services, The University of the Witwatersrand, Geological Survey of Namibia, Geological Survey of Botswana, Rio Tinto Mining and Exploration, BHP Billiton, Council for Scientific and Industrial Research of South Africa, and ABB Sweden for the Namibian Power Corporation. Other contributors to the SAMTEX project in terms of instruments and instrumentations are Phoenix Geophysics, the Geological Survey of Canada, and the U.S. Electromagnetic Studies of Continents consortium (EMSOC). Special thanks to the SAMTEX funding sponsors: the Continental Dynamics programme of the U.S. National Science Foundation (grant number: EAR0455242 and EAR-0309584), the South African Department of Science and Technology, and Science Foundation Ireland (Ireland, grant 05/RFP/GEO001). Also, thanks to the farmers and landowners for allowing access to their properties for MT station deployment.

Special acknowledgement to the providers of the various facilities and codes used for this study. For the visualization of the results, figures, and illustrations, we used the MTPy (Kirkby et al., 2019; Krieger & Peacock, 2014) and the Generic Mapping Tools (GMT) (Wessel et al., 2019). We used the ModEM codes (Egbert & Kelbert, 2012; Kelbert et al., 2014) for the 3-D MT inversion process. Computational resources from the Faculty of Geoinformation and Earth Observation (ITC), University of Twente and the Dutch National Supercomputing Facilities (Grant Number: EINF-1468), were used for the 3-D MT inversion computations. The authors would like to appreciate Dr. Naser Meqbel for the support on the use of ModEM software. Special thanks to Prof. Michael Becken for fruitful discussions and suggestions.

Finally, the results presented in the article first appeared in the MSc thesis of Mr. Stephen Akinremi (Akinremi, 2021) at the Department of Earth Systems Analysis, Faculty of Geo-Information Science and Earth Observation (ITC) of the University of Twente, The Netherlands. Mr. Akinremi has received funding through the ITC Foundation Special Scholarship (ITCFSS) for his study.

References

Adetunji, A., Ferguson, I., & Jones, A. (2015). Reexamination of magnetotelluric responses and electrical anisotropy of the lithospheric mantle in the Grenville Province, Canada. *Journal of Geophysical Research*, 3782–3803. https://doi.org/10.1002/2015JB012608.Received

Akinremi, S. (2021). *Crustal and upper mantle imaging of Botswana using magnetotelluric method* (Faculty of Geoinformation Science and Earth Observation (ITC) of the University of Twente). Retrieved from https://essay.utwente.nl/88633/

Becken, M., & Burkhardt, H. (2004). An ellipticity criterion in magnetotelluric tensor analysis. *Geophysical Journal International*, *159*(1), 69–82. https://doi.org/10.1111/j.1365-246X.2004.02376.x

Becken, M., Ritter, O., & Burkhardt, H. (2008). Mode separation of magnetotelluric responses in three-dimensional environments. *Geophysical Journal International*, *172*(1), 67–86. https://doi.org/10.1111/j.1365-246X.2007.03612.x

Begg, G. C., Griffin, W. L., Natapov, L. M., O'Reilly, S. Y., Grand, S. P., O'Neill, C. J., … Bowden, P. (2009). The lithospheric architecture of Africa: Seismic tomography, mantle petrology, and tectonic evolution. *Geosphere*, *5*(1), 23–50. https://doi.org/10.1130/GES00179.1

Bibby, H. M., Caldwell, T. G., & Brown, C. (2005). Determinable and non-determinable parameters of galvanic distortion in magnetotellurics. *Geophysical Journal International*, *163*(3), 915–930. https://doi.org/10.1111/j.1365-246X.2005.02779.x

Booker, J. R. (2014). The Magnetotelluric Phase Tensor: A Critical Review. *Surveys in Geophysics*, *35*(1), 7–40. https://doi.org/10.1007/s10712-013-9234-2

Brandt, M. B. C., Grand, S. P., Nyblade, A. A., & Dirks, P. H. G. M. (2011). Upper mantle seismic structure beneath Southern Africa : constraints on the buoyancy supporting the African superswell. *Pure and Applied Geophysics*, (March). https://doi.org/10.1007/s00024-011-0361-8

Caldwell, T. G., Bibby, H. M., & Brown, C. (2004). The magnetotelluric phase tensor. *Geophysical Journal International*, *158*(2), 457–469. https://doi.org/10.1111/j.1365-246X.2004.02281.x

Campany, J., Jones, A. G., Rath, V., Vozar, J., & Meqbel, N. (2016). The advantages of complementing MT profiles in 3-D environments with geomagnetic transfer function and interstation horizontal magnetic transfer function data : results from a synthetic case study. *Geophysical Journal International*, 1818–1836. https://doi.org/10.1093/gji/ggw357

Carlson, R. W., Grove, T. L., De Wit, M. J., & Gurney, J. J. (1996). Program to study crust and mantle of the Archean craton in southern Africa. *Eos, Transaction, American Geophysical Union*, *77*(29), 273–277. https://doi.org/10.1029/96eo00194

Chave, A. D., & Jones, A. G. (2012). The magnetotelluric method: Theory and practice. In *The Magnetotelluric Method: Theory and Practice*. https://doi.org/doi:10.1017/CBO9781139020138.004

Cherevatova, M., Smirnov, M. Y., Jones, A. G., Pedersen, L. B., Becken, M., Biolik, M., …

Smirnov, M. (2015). Magnetotelluric array data analysis from north-west Fennoscandia. *Tectonophysics*, *653*, 1–19. https://doi.org/10.1016/j.tecto.2014.12.023

Chisenga, C., Jianguo, Y., Fadel, I., Meijde, M. van der, & Atekwana, E. A. (2020). Updated tectonic terrane boundaries of Botswana determined from gravity and aeromagnetic data. *Episodes, Journal of International Geosciences*, 1–15. https://doi.org/10.18814/epiiugs/2020/020054

Chisenga, C., Van der Meijde, M., Yan, J., Fadel, I., Atekwana, E. A., Steffen, R., & Ramotoroko, C. (2020). Gravity derived crustal thickness model of Botswana: Its implication for the Mw 6.5 April 3, 2017, Botswana earthquake. *Tectonophysics*, *787*(May). https://doi.org/10.1016/j.tecto.2020.228479

Comeau, M. J., Becken, M., Käufl, J. S., Grayver, A. V., Kuvshinov, A. V., Tserendug, S., … Demberel, S. (2020). Evidence for terrane boundaries and suture zones across Southern Mongolia detected with a 2-dimensional magnetotelluric transect. *Earth, Planets and Space*, *72*(1). https://doi.org/10.1186/s40623-020-1131-6

Egbert, G. D., & Kelbert, A. (2012). Computational recipes for electromagnetic inverse problems. *Geophysical Journal International*, *189*(1), 251–267. https://doi.org/10.1111/j.1365-246X.2011.05347.x

Evans, R. L., Elsenbeck, J., Zhu, J., Abdelsalam, M. G., Sarafian, E., Mutamina, D., … Jones, A. G. (2019). Structure of the Lithosphere Beneath the Barotse Basin, Western Zambia, From Magnetotelluric Data. *Tectonics*, *38*(2), 666–686. https://doi.org/10.1029/2018TC005246

Evans, Rob L., Jones, A. G., Garcia, X., Muller, M., Hamilton, M., Evans, S., … Hutchins, D. (2011). Electrical lithosphere beneath the Kaapvaal craton, southern Africa. *Journal of Geophysical Research: Solid Earth*, *116*(4), 1–16. https://doi.org/10.1029/2010JB007883

Fadel, I. (2018). *Crustal and upper mantle structure of Botswana : is Botswana rifting?* (Faculty of Geoinformation Science and Earth Observation (ITC)-University of Twente). https://doi.org/dx.doi.org/10.3990/1.9789036544641

Fadel, I., Paulssen, H., van der Meijde, M., Kwadiba, M., Ntibinyane, O., Nyblade, A., & Durrheim, R. (2020). Crustal and Upper Mantle Shear Wave Velocity Structure of Botswana: The 3 April 2017 Central Botswana Earthquake Linked to the East African Rift System. *Geophysical Research Letters*, *47*(4). https://doi.org/10.1029/2019GL085598

Fadel, I., van der Meijde, M., & Paulssen, H. (2018). Crustal Structure and Dynamics of Botswana. *Journal of Geophysical Research: Solid Earth*, *123*(12), 10,659-10,671. https://doi.org/10.1029/2018JB016190

Fouch, M. J., James, D. E., VanDecar, J. C., & van der Lee, S. (2004). Mantle seismic structure beneath the Kaapvaal and Zimbabwe Cratons. *South African Journal of Geology*, *107*(1–2), 33–44. https://doi.org/10.2113/107.1-2.33

Gao, S. S., Liu, K. H., Reed, C. A., Yu, Y., Massinque, B., Mdala, H., … Reusch, A. M. (2013). Seismic Arrays to Study African Rift Initiation. *Eos, American Geophysical Union*, *94*(24), 213–214.

Gardonio, B., Jolivet, R., Calais, E., & Leclère, H. (2018). The April 2017 Mw6.5 Botswana Earthquake: An Intraplate Event Triggered by Deep Fluids. *Geophysical Research Letters*, *45*(17), 8886–8896. https://doi.org/10.1029/2018GL078297

Groom, R. W., & Bailey, R. C. (1991). Analytic investigations of the effects of near-surface three-dimensional galvanic scatterers on MT tensor decompositions. *Geophysics*, *56*(4), 496–518. https://doi.org/10.1190/1.1443066

Haddon, I. G. (2005). The Sub-Kalahari Geology and Tectonic Evolution of the Kalahari Basin, Southern Africa. *PhD Thesis, Faculty of Science, University of the Witwatersrand, Johannesburg*, 1–360.

Hutchins, D. G., & Reeves, C. V. (1980). Regional geophysical exploration of the Kalahari in Botswana. *Test Tectonophysics*, *69*(3–4), 201–220. https://doi.org/10.1016/0040-1951(80)90211-5

Jones, A.G., Evans, R. L., Muller, M. R., Hamilton, M. P., Miensopust, M. P., Garcia, X., … Team, T. S. (2009). The SAMTEX Experiment: Overview and Preliminary Results. *11th SAGA Biennial Technical Meeting and Exhibition*. https://doi.org/10.3997/2214-4609-pdb.241.jones_paper1

Jones, Alan G., & Garcia, X. (2006). Electrical resistivity structure of the Yellowknife River Fault zone and surrounding region. *Geological Association of Canada, Mineral Deposits Division*, *3*(3), 126–141.

Jones, Alan G., Ledo, J., & Ferguson, I. J. (2005). Electromagnetic images of the Trans-Hudson orogen: The North American Central Plains anomaly revealed. *Canadian Journal of Earth Sciences*, *42*(4), 457–478. https://doi.org/10.1139/e05-018

Jones, Alan G, Chave, A. D., Egbert, G., & Auld, D. O. N. (1989). A comparison of techniques for magnetotelluric response function estimation. *Journal of Geophysical Research*, *94*, 201–213.

Jones, Alan G, Evans, R. L., Muller, M. R., Hamilton, M. P., Miensopust, M. P., Garcia, X., … Team, T. S. (2009). Area selection for diamonds using magnetotellurics : Examples from southern Africa. *LITHOS*, *112*, 83–92. https://doi.org/10.1016/j.lithos.2009.06.011

Jones, M. Q. W. (1988). Heat flow in the Witwatersrand basin and environs and its significance for the South African shield geotherm and lithosphere thickness. *Journal of Geophysical Research*, *93*(B4), 3243–3260. https://doi.org/10.1029/JB093iB04p03243

Kelbert, A., Meqbel, N., Egbert, G. D., & Tandon, K. (2014). ModEM: A modular system for inversion of electromagnetic geophysical data. *Computers and Geosciences*, *66*, 40–53. https://doi.org/10.1016/j.cageo.2014.01.010

Key, R. M., & Ayres, N. (2000). The 1998 edition of the National Geological Map of Botswana. *Journal of African Earth Sciences*, *30*(3), 427–451. https://doi.org/10.1016/S0899-5362(00)00030-0

Khoza, D., Jones, A. G., Muller, M. R., Evans, R. L., Webb, S. J., & Miensopust, M. (2012). Tectonic model of the Limpopo belt: constraints from magnetotelluric data. *Precambrian*

Research, *226*, 143–156. https://doi.org/http://dx.doi.org/10.1016/j.precamres.2012.11.016

Khoza, D., Jones, A., Muller, M., Evans, R., Miensopust, M., & Webb, S. (2013). Lithospheric structure of an Archean craton and adjacent mobile belt revealed from 2-D and 3-D inversion of magnetotelluric data: Example from southern Congo craton in northern Namibia. *Journal of Geophysical Research: Solid Earth*, *118*(8), 4378–4397. https://doi.org/10.1002/jgrb.50258

Kinabo, B. D., Atekwana, E. A., Hogan, J. P., Modisi, M. P., Wheaton, D. D., & Kampunzu, A. B. (2007). Early structural development of the Okavango rift zone , NW Botswana. *Journal of African Earth Sciences*, *48*, 125–136. https://doi.org/10.1016/j.jafrearsci.2007.02.005

Kinabo, B. D., Hogan, J. P., Atekwana, E. A., Abdelsalam, M. G., & Modisi, M. P. (2008). Fault growth and propagation during incipient continental rifting: Insight from a combined aeromagnetic and Shuttle Radar Topography Mission digital elevation model investigation of the Okavango Rift Zone, northwest Botswana. *Tectonics*, *27*(3), 1–16. https://doi.org/10.1029/2007TC002154

Kirkby, A., Zhang, F., Peacock, J., Hassan, R., & Duan, J. (2019). The MTPy software package for magnetotelluric data analysis and visualisation. *Journal of Open Source Software*, *4*(37), 1358. https://doi.org/10.21105/joss.01358

Kolawole, F., Atekwana, E. A., Malloy, S., Stamps, D. S., Grandin, R., Abdelsalam, M. G., … Shemang, E. M. (2017). Aeromagnetic, gravity, and Differential Interferometric Synthetic Aperture Radar analyses reveal the causative fault of the 3 April 2017 Mw 6.5 Moiyabana, Botswana, earthquake. *Geophysical Research Letters*, *44*(17), 8837–8846. https://doi.org/10.1002/2017GL074620

Krieger, L., & Peacock, J. R. (2014). MTpy: A Python toolbox for magnetotellurics. *Computers and Geosciences*, *72*, 167–175. https://doi.org/10.1016/j.cageo.2014.07.013

Ledo, J. (2005). 2-D versus 3-D magnetotelluric data interpretation. *Surveys in Geophysics*, *26*(5), 511–543. https://doi.org/10.1007/s10712-005-1757-8

Ledo, J., Queralt, P., Martí, A., & Jones, A. G. (2002). Two-dimensional interpretation of three-dimensional magnetotelluric data: An example of limitations and resolution. *Geophysical Journal International*, *150*(1), 127–139. https://doi.org/10.1046/j.1365-246X.2002.01705.x

Leseane, K., Atekwana, E. A., Mickus, K. L., Abdelsalam, M. G., Shemang, E. M., & Atekwana, E. A. (2015). Thermal perturbations beneath the incipient Okavango Rift Zone, northwest Botswana. *Journal of Geophysical Research: Solid Earth*, 3782–3803. https://doi.org/10.1002/2014JB011029

McCourt, S., Armstrong, R. A., Jelsma, H., & Mapeo, R. B. M. (2013). New U-Pb SHRIMP ages from the Lubango region, SW Angola: Insights into the Palaeoproterozoic evolution of the Angolan Shield, southern Congo Craton, Africa. *Journal of the Geological Society*, *170*(2), 353–363. https://doi.org/10.1144/jgs2012-059

Meqbel, N. M., Egbert, G. D., Wannamaker, P. E., Kelbert, A., & Schultz, A. (2014). Deep electrical resistivity structure of the northwestern U.S. derived from 3-D inversion of USArray magnetotelluric data. *Earth and Planetary Science Letters*, *402*(C), 290–304.

https://doi.org/10.1016/j.epsl.2013.12.026

Midzi, V., Saunders, I., Manzunzu, B., Kwadiba, M. T., Jele, V., Mantsha, R., … Zulu, B. S. (2018). The 03 April 2017 Botswana M6.5 earthquake: Preliminary results. *Journal of African Earth Sciences*, *143*, 187–194. https://doi.org/10.1016/j.jafrearsci.2018.03.027

Miensopust, M. P., Jones, A. G., Muller, M. R., Garcia, X., & Evans, R. L. (2011). Lithospheric structures and Precambrian terrane boundaries in northeastern Botswana revealed through magnetotelluric profiling as part of the Southern African Magnetotelluric Experiment. *Journal of Geophysical Research*, *116*, 1–21. https://doi.org/10.1029/2010JB007740

Modisi, M. P. (2000). Fault system at the southeastern boundary of the Okavango Rift, Botswana. *Journal of African Earth Sciences*, *30*(3), 569–578. https://doi.org/10.1016/S0899-5362(00)00039-7

Modisi, M. P., Atekwana, E. A., Kampunzu, A. B., & Ngwisanyi, T. H. (2000). Rift kinematics during the incipient stages of continental extension: Evidence the nascent Okavango rift basin, Northwest Botswana. *Geology*, *28*(10), 939–942. https://doi.org/10.1130/0091-7613(2000)28<939:RKDTIS>2.0.CO;2

Moorkamp, M., Fishwick, S., Walker, R. J., & Jones, A. G. (2019). Geophysical evidence for crustal and mantle weak zones controlling intra-plate seismicity – the 2017 Botswana earthquake sequence. *Earth and Planetary Science Letters*, *506*, 175–183. https://doi.org/10.1016/j.epsl.2018.10.048

Muller, M. R., Jones, A. G., Evans, R. L., Grütter, H. S., Hatton, C., Garcia, X., … Wasborg, J. (2009). Lithospheric structure, evolution and diamond prospectivity of the Rehoboth Terrane and western Kaapvaal Craton, southern Africa: Constraints from broadband magnetotellurics. *Lithos*, *112*, 93–105. https://doi.org/10.1016/j.lithos.2009.06.023

Niblett, E. R., & Sayn-wittgenstein, C. (1960). Variation of electrical conductivity with depth by the magnetotelluric method. *Geophysics*.

Nyblade, A., Dirks, P., Durrheim, R., Webb, S., Jones, M., Cooper, G., & Graham, G. (2008). AfricaArray: Developing a geosciences workforce for Africa's natural resource sector. *The Leading Edge*, *27*(10), 1358–1361. https://doi.org/10.1190/1.2996547

Ortiz, K., Nyblade, A., Meijde, M. Van Der, Paulssen, H., Kwadiba, M., Ntibinyane, O., … Homman, K. (2019). Upper mantle P and S wave Velocity structure of the Kalahari Craton and surrounding Proterozoic terranes , southern Africa Geophysical Research Letters. *Geophysical Research Letters*, 9509–9518. https://doi.org/10.1029/2019GL084053

Ozaydin, S., Selway, K., Griffin, W. L., & Moorkamp, M. (2021). Probing the southern African lithosphere with magnetotellurics , Part II , linking electrical conductivity , composition and tectono-magmatic. *Earth and Space Science OPen Archive*, (September). https://doi.org/10.1002/essoar.10507861.1

Panza, G. F., Peccerillo, A., Aoudia, A., & Farina, B. (2006). Geophysical and petrological modelling of the structure and composition of the crust and upper mantle in complex geodynamic settings: the Tyrrhenian sea and surroundings. *Earth Science Reviews*.

https://doi.org/10.1016/j.earscirev.2006.08.004

Pastier, A. M., Dauteuil, O., Murray-Hudson, M., Moreau, F., Walpersdorf, A., & Makati, K. (2017). Is the Okavango Delta the terminus of the East African Rift System? Towards a new geodynamic model: Geodetic study and geophysical review. *Tectonophysics*, *712–713*, 469–481. https://doi.org/10.1016/j.tecto.2017.05.035

Pretorius, D. A. (1984). *The Kalahari Foreland, its marginal troughs and overthrust belts, and the regional structure of Botswana*. Johannesburg, South Africa: University of Witwatersrand.

Reeves, C. V. (1972). Rifting in the Kalahari? *Nature*, 95–96. https://doi.org/10.1038/237095a0

Reeves, C. V., & Hutchins, D. G. (1982). A progress report on the geophysical exploration of the Kalahari in Botswana. *Geoexploration*, *20*(3–4), 209–224. https://doi.org/10.1016/0016-7142(82)90022-9

Robertson, K., Thiel, S., & Meqbel, N. (2020). Quality over quantity : on workflow and model space exploration of 3D inversion of MT data. *Earth, Planets and Space*. https://doi.org/10.1186/s40623-019-1125-4

Simpson, F., & Bahr, K. (2005). *Practical magnetotellurics*. Cambridge, UK: Cambridge University Press.

Smith, J. T. (1995). Understanding telluric distortion matrices. *Geophysical Journal International*, *122*(1), 219–226. https://doi.org/10.1111/j.1365-246X.1995.tb03549.x

Sobh, M., Gerhards, C., & Fadel, I. (2021). Mapping the thermal structure of southern Africa from Curie depth estimates based on wavelet analysis of magnetic data with uncertainties. *Geochemistry, Geophysics, Geosystems*, 1–29. https://doi.org/10.1029/2021GC010041

Telford, W. M., Geldart, L. P., & Sheriff, R. E. (2004). *Applied Geophysics* (Second). Cambridge, UK: Cambridge University Press.

Thomas, R. J., von Veh, M. W., & McCourt, S. (1993). The tectonic evolution of southern Africa: an overview. *Journal of African Earth Sciences*, *16*(1–2), 5–24. https://doi.org/10.1016/0899-5362(93)90159-N

Van Schijndel, V., Cornell, D. H., Frei, D., Simonsen, S. L., & Whitehouse, M. J. (2014). Crustal evolution of the rehoboth province from archaean to mesoproterozoic times: Insights from the rehoboth basement inlier. *Precambrian Research*, *240*, 22–36. https://doi.org/10.1016/j.precamres.2013.10.014

Van Schijndel, V., Cornell, D. H., Hoffmann, K. H., & Frei, D. (2011). Three episodes of crustal development in the Rehoboth Province, Namibia. *Geological Society Special Publication*, *357*(1), 27–47. https://doi.org/10.1144/SP357.3

Wannamaker, P. E., Hasterok, D. P., Johnston, J. M., Stodt, J. A., Hall, D. B., Sodergren, T. L., … Unsworth, M. J. (2008). Lithospheric dismemberment and magmatic processes of the Great Basin-Colorado Plateau transition, Utah, implied from magnetotellurics. *Geochemistry, Geophysics, Geosystems*, *9*(5), 1–38. https://doi.org/10.1029/2007GC001886

Wessel, P., Luis, J. F., Uieda, L., Scharroo, R., Wobbe, F., Smith, W. H. F., & Tian, D. (2019). The Generic Mapping Tools Version 6. *Geochemistry, Geophysics, Geosystems*, *20*(11), 5556–5564. https://doi.org/10.1029/2019GC008515

White-Gaynor, A. L., Nyblade, A. A., Durrheim, R. J., Raveloson, R., van der Meijde, M., Fadel, I., … Sitali, M. (2021). Shear-Wave Velocity Structure of the Southern African Upper Mantle: Implications for Craton Structure and Plateau Uplift. *Geophysical Research Letters*, *48*(7), 1–10. https://doi.org/10.1029/2020GL091624

Wright, J. A., & Hall, J. (1990). Deep Seismic profiling in the Nosop Basin, Botswana: cratons, mobile belts and sedimentary basins. *Tectonophysics*, *173*(1–4), 333–343. https://doi.org/10.1016/0040-1951(90)90228-Z

Yu, Y., Gao, S. S., Moidaki, M., Reed, C. A., & Liu, K. H. (2015). Seismic anisotropy beneath the incipient Okavango rift : Implications for rifting initiation. *Earth and Planetary Science Letters*, *430*, 1–8. https://doi.org/10.1016/j.epsl.2015.08.009

Yu, Youqiang, Gao, S. S., Moidaki, M., Reed, C. A., & Liu, K. H. (2015). Seismic anisotropy beneath the incipient Okavango rift: Implications for rifting initiation. *Earth and Planetary Science Letters*, *430*, 1–8. https://doi.org/10.1016/j.epsl.2015.08.009

Yu, Youqiang, Liu, K. H., Moidaki, M., Reed, C. A., & Gao, S. S. (2015). No thermal anomalies in the mantle transition zone beneathe an incipient continental rift : evidence from the first receiver function study across the Okavango Rift Zone, Botswana. *Geophysical Journal International*, 1407–1418. https://doi.org/10.1093/gji/ggv229

Yu, Youqiang, Liu, K. H., Reed, C. A., Moidaki, M., Mickus, K., Atekwana, E. A., & Gao, S. S. (2015). A joint receiver function and gravity study of crustal structure beneath the incipient Okavango Rift , Botswana. *American Geophysical Union*. https://doi.org/10.1002/2015GL065811.Abstract

Supplementary Material

1 MT Data Analysis

1.1 Data Resolution Depth

The MT method is capable of imaging great depths (up to the upper mantle) significantly more than other active source electromagnetic methods. The depth of penetration of the MT method is dependent on the resistivity of the medium and the period of sounding. The higher the resistivity of the medium, the higher the depth of penetration and the lower the frequency of measurement, the higher the penetration depth. Electromagnetic skin depth is a measure of the depth of the maximum sensitivity of the measured field (Simpson & Bahr, 2005). Long period (low frequency) MT data can be used to image greater depth in the subsurface (up to the mantle). This is because long period electromagnetic waves attenuate slower than short period waves; hence the former penetrates deeper into the Earth.

We carried out depth resolution analysis on the data to investigate the depth to which the MT response is sensitive and can be reliably interpreted. The depths of penetration were calculated using the Niblett-Bostick transformation (Niblett & Sayn-wittgenstein, 1960) to account for variation in depth of penetration for MT sites at similar frequencies. The results of the depth of penetration estimates of the MT data coverage in Botswana for representative periods of 100, 250, 500, and 1,000 seconds are shown in Figure S1. The red colour indicate high depth of penetration of the MT data (between 200 km – 250 km), while the blue colour shows shallower depth of penetration (< 120 km). There is a general increase in the depth of penetration of the MT sites as the period increases, which is evident by more MT sites with high depth of penetration at periods of 500 seconds and 1,000 seconds. At the period of 100 seconds, there are some missing MT sites in the result, whose shortest periods are greater than 100 seconds. The disappearance of some MT sites in the result at longer periods of 500 seconds and 1,000 seconds is due to the lack of long-period data at those sites.

The depth of penetration of the MT data is dependent on the period of recording the MT data and the bulk resistivity of the Earth medium. High bulk resistivity in the subsurface allows for a high depth of penetration of the MT data. Spatially, MT sites that have a relatively higher depth of penetration correspond to stations above cratonic provinces, which have high bulk resistivity values as revealed in the electrical conductivity model. For example, at the period of 250 seconds, higher depth up to 250 km depth is sensed by MT stations above the Congo Craton, Zimbabwe Craton, Rehoboth Province, and Kaapvaal Craton in the northwest, east, west, and south of Botswana, respectively. From the results, the MT data cover in Botswana used in this study can image up to 200 km depth in the subsurface, with 68% of the MT sites having periods above 1,000 seconds.

As the depth of penetration of the MT data becomes higher, the horizontal adjustment length, which is the lateral distance that the MT data is sensitive to increases. At the various depth of penetration of the MT data, the horizontal adjustment length is approximately 2 – 3 times the value of the penetration depth (Simpson & Bahr, 2005). It is then possible to image any subsurface structure that is off the MT data site within the horizontal adjustment length range at a given depth. The results of the 3D country-wide model of this study are discussed along profiles on top or in the near proximity of the MT stations to address the shortcoming of the small horizontal adjustment distance at short periods.

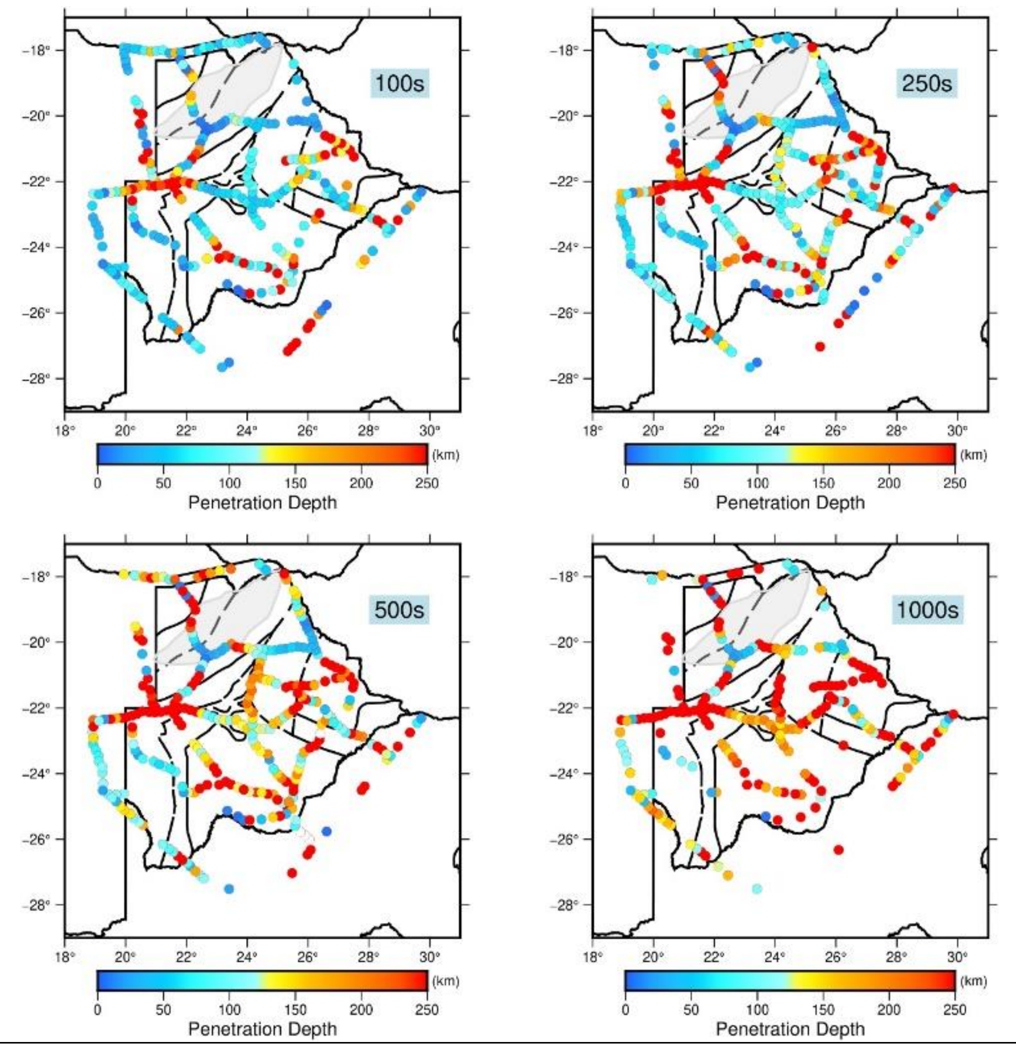

Figure S1: Depth of penetration of the MT data at periods of 100, 250, 500, and 1,000 seconds. The MT sites are represented in circles and the corresponding depths of penetration are indicated by the colour.

1.2 Data Dimensionality

Dimensionality analysis of MT data is an essential step to ensure that the subsurface structure has the same dimensionality as the modelling approach used for the data. In a case where the dimensionality of the MT data is higher than the dimension in which the data is modelled or interpreted (e.g., a 1-D interpretation of a 2-D or 3-D structure), dimensionality distortion occurs in the model, causing inaccurate and erroneous interpretation (Ledo, 2005; Ledo et al., 2002). We carried dimensionality analysis of the data to understand the dimensionality captured in the MT data. The dimensionality analysis was done based on the phase tensor, which is not affected by galvanic distortion as described by Bibby et al. (2005), Booker (2014) and Caldwell et al. (2004). The skew value and ellipticity parameters of the phase tensor were used to analyze the dimensionality. The skew value is a ratio of the amplitudes of the sum of diagonal components to the sum of the off-diagonal components of the impedance tensor. High skew values of the phase tensor greater than 6 ^{o} indicate 3-D effects, skew values of 0 ^{o} indicate 2-D data, and lower skew values indicate 1-D subsurface structure (Cherevatova et al., 2015; Comeau et al., 2020). The ellipticity of the phase tensor is defined by the ratio of the amplitudes of the sum of diagonal components to the sum of the off-diagonal components of the impedance phase. When the phase tensor is a circle, it indicates 1-D subsurface, while the elliptical phase tensor represents 2-D or 3-D effects in the conductivity distribution (Becken & Burkhardt, 2004; Bibby et al., 2005). A more in-depth description of the parameters of the impedance tensor can be found in Bibby et al. (2005) and Booker (2014).

The results of the phase tensor dimensionality analysis for twelve representative profiles from major geological provinces in Botswana are presented as pseudo section plots in Figure S2, S3, and S4. The pseudo sections are plotted as circles and ellipses, while the colour indicates the skew value of the phase tensor. High skew values greater than 6 ^{o}, which are shown in light to dark brown colour, indicate 3-D effects in the data. Also, when the phase tensor's shape is circular, it indicates a 1-D structure, while elliptical phase tensors show 2-D or 3-D effects in the data.

The results of the phase tensor analysis show the presences of 3-D components in the MT data. There is 3-D resistivity structure in most of the MT data sites, which is evident by the high skew values (> 6 ^{o}) and elliptical nature of the phase tensor for many of the MT sites, hence the need to model the data in 3-D. The result of this analysis confirms the 3-D nature of the terrane beneath Botswana as reflected in the MT data. The previous MT studies done in Botswana using the SAMTEX data (e.g., Miensopust et al., (2011), Muller et al., (2009), and Khoza et al., (2012)) confirmed the presence of 3-D components in the MT data. There exist multiple principal geoelectric strike directions in the MT data, which is indicative of 3-D structure (e.g., Miensopust et al., (2011), Muller et al., (2009), and Khoza et al., (2012)). For this study, we inverted the MT data in 3-D without need for assumption of geoelectric strike directions, which is required for 2-D modelling.

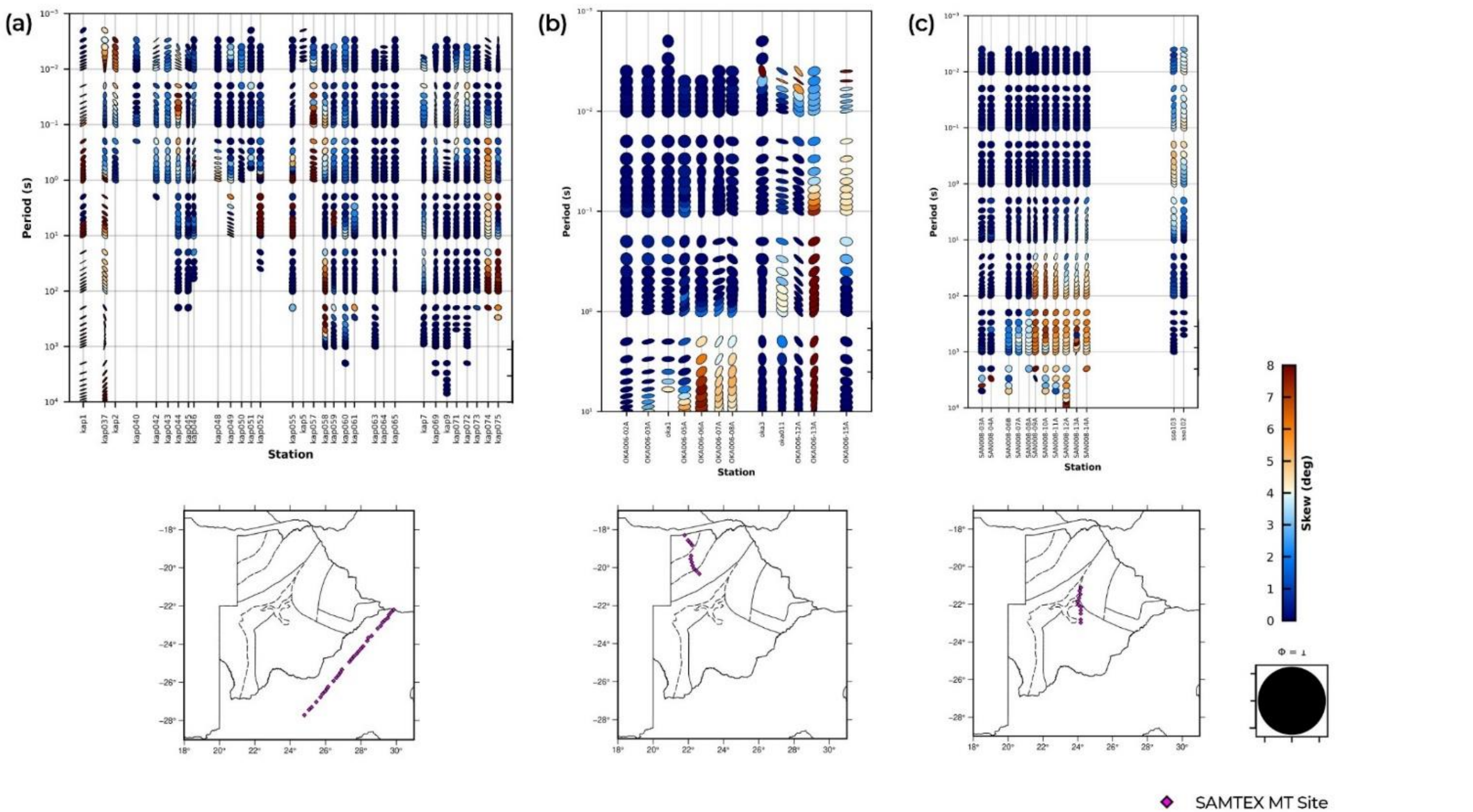

Figure S2: Phase tensor analysis result for three representative profiles. (a-c) Phase tensor ellipses for all periods in MT sites plotted. The corresponding profiles' locations are also shown below each phase tensor ellipse plot with the MT stations' locations as purple diamonds. The phase tensors are plotted left-right or top to bottom along the profiles. The pseudo sections are plotted as circles and ellipses, while the colour indicates the skew value of the phase tensor.

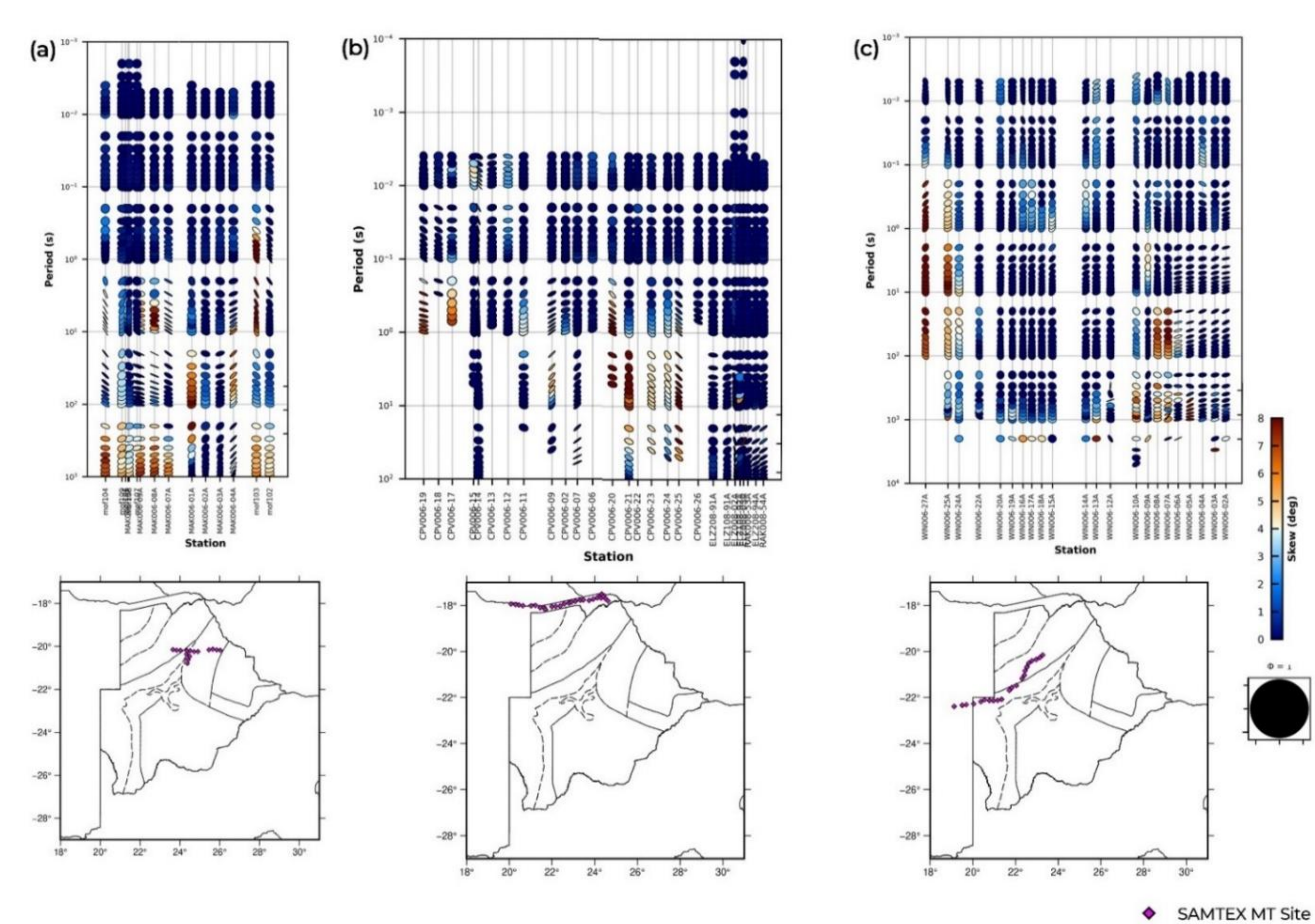

Figure S3: Phase tensor analysis result for three representative profiles. (a-c) Phase tensor ellipses for all periods in MT sites plotted. The corresponding profiles' locations are shown also below each phase tensor ellipse plot with the MT stations' locations as purple diamonds. The phase tensors are plotted left-right or top to bottom along the profiles. The pseudo sections are plotted as circles and ellipses, while the color indicates the skew value of the phase tensor.

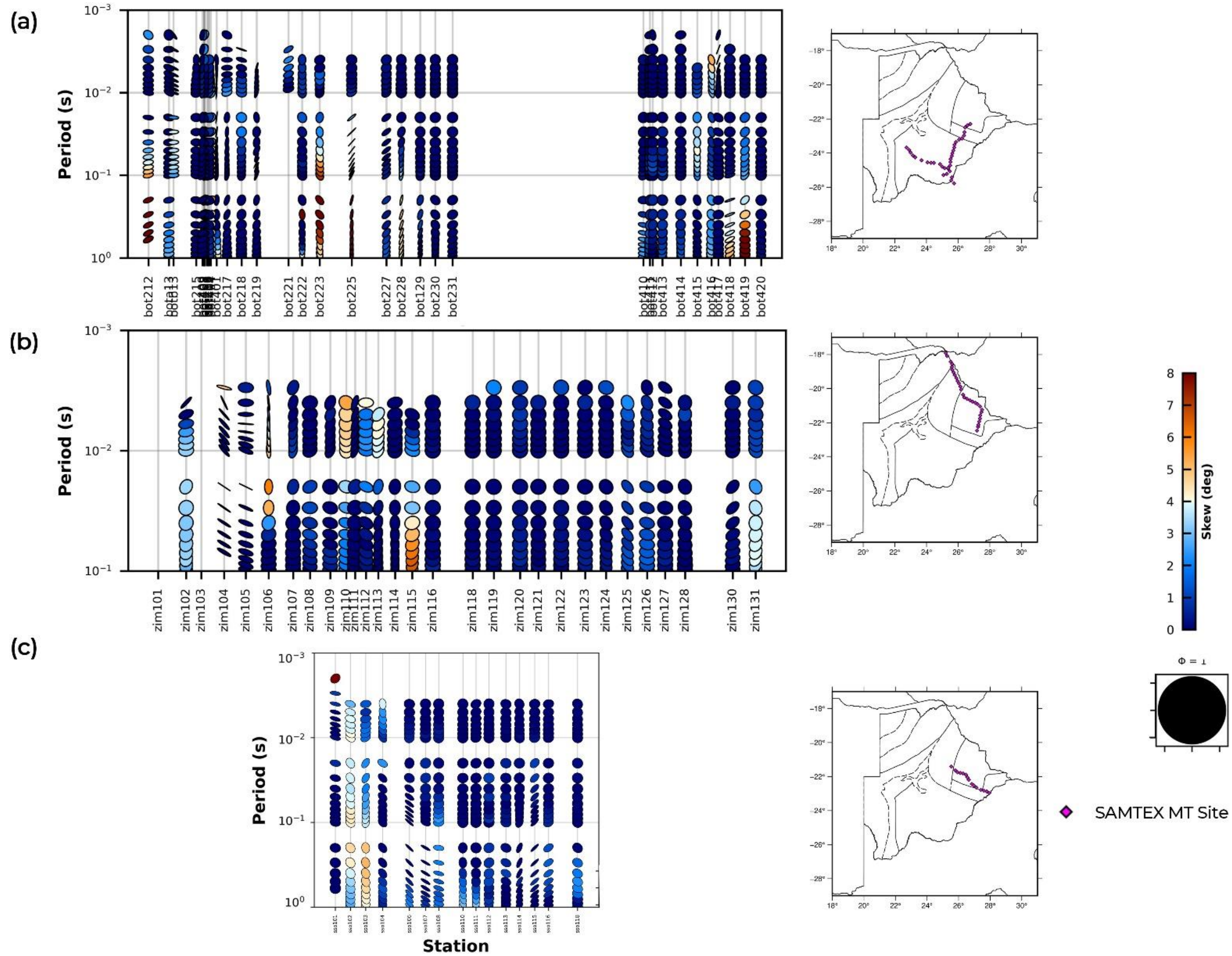

Figure S4: Phase tensor analysis result for three representative profiles. (a-c) Phase tensor ellipses for all periods in MT sites plotted. The corresponding profiles' locations are shown also below each phase tensor ellipse plot with the MT stations' locations as purple diamonds. The phase tensors are plotted left-right or top to bottom along the profiles. The pseudo sections are plotted as circles and ellipses, while the color indicates the skew value of the phase tensor.

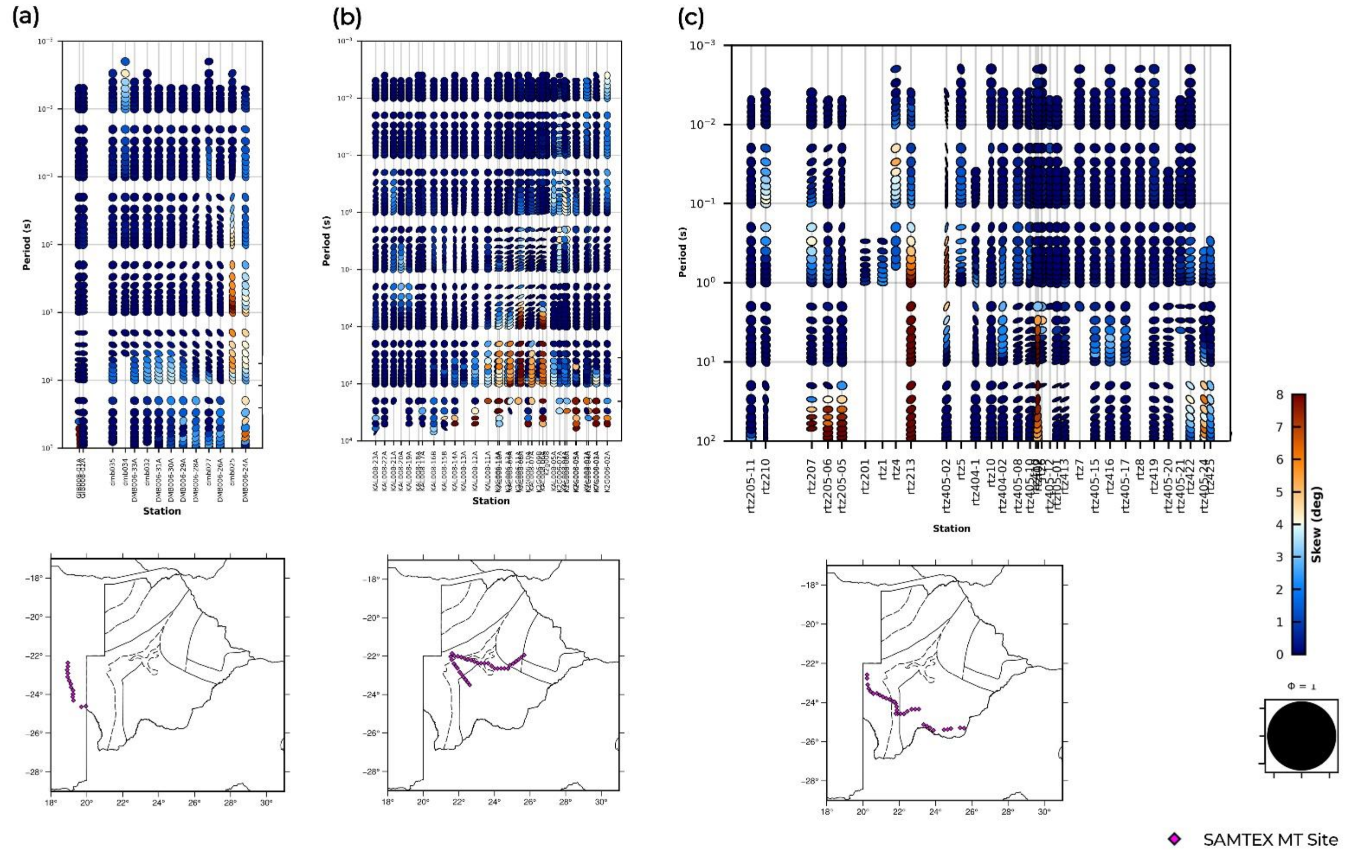

Figure S5: Phase tensor analysis result for three representative profiles. (a-c) Phase tensor ellipses for all periods in MT sites plotted. The corresponding profiles' locations are shown also below each phase tensor ellipse plot with the MT stations' locations as purple diamonds. The phase tensors are plotted left-right or top to bottom along the profiles. The pseudo sections are plotted as circles and ellipses, while the color indicates the skew value of the phase tensor.

2 Sensitivity Tests

2.1 ModEM Inversion Initial Damping Parameter

The ModEM codes allow the user to control the inversion process with the initial damping parameter and inversion computation stopping criterion (Kelbert et al., 2014). The damping parameter controls how the model fits the data progressively in the inversion process (Robertson et al., 2020). As part of this study, a sensitivity test was carried out to investigate how the initial damping parameter affects the resultant model. We used a subset of the MT data consisting of 28 stations in central Botswana for this test to ensure shorter processing time (Figure S6). Initial damping parameters of 1, 10, 100 and 1,000 were tested. We compare the model misfits for the four resultant models (Table S1).

From the results, the nRMS values for the four models are similar. To further gain insight into the resultant models, depth sections corresponding to 7 km, 31 km, and 49 km for the four different models were compared (Figure S6a). Visually, the plan view of depth sections when compared for the four models look similar. However, there is a difference in the number of NLCG iterations required for the model to converge for the different initial damping parameters used. Higher initial damping parameters of 100 and 1,000 took longer NLCG iterations and computation time to achieve convergence of the inversion. The choice of the initial damping parameter has little influence on the resultant model and data misfit. The observations from this sensitivity test are consistent with the results from model space exploration with the Australian Lithospheric Architecture Magnetotelluric Project data using the ModEM codes done by Robertson et al. (2020). For the Botswana country-wide 3-D electrical conductivity modelling, an initial damping parameter of 10 was used to reduce the computing time.

Table S1: Summary of the nRMS for Initial Damping Parameter Sensitivity Test

Initial Damping Parameter	Overall nRMS	Number of NLCG Iteration
1	2.044264	81
10	2.101267	80
100	2.085736	110
1000	2.069875	122

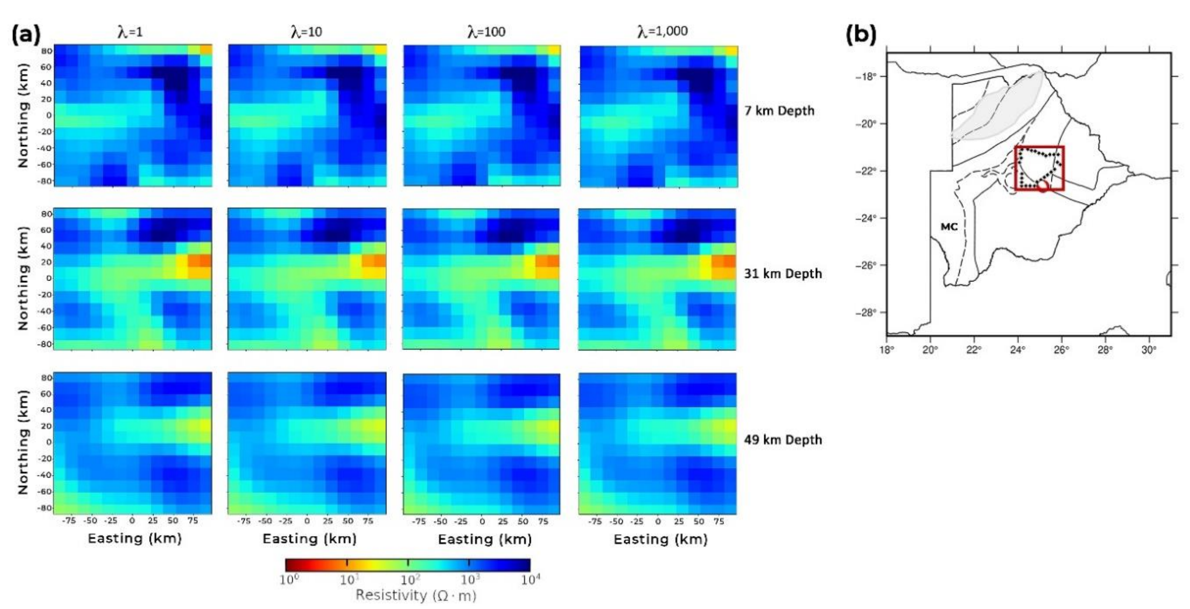

Figure S6: Plan view of electrical conductivity model depth slices at 7 km, 31 km, and 49 km for initial damping parameters of 1, 10, 100, and 1,000 (b) Location Map with the MT stations location as black dots. Red bounding box = location of models presented in (a).

2.2 Model Grid Resolution

Model grid resolution determination is an important step in 3-D MT inversion. The decision of the size of the model grid is usually based on the interstation distances of the stations and a balanced choice between two factors; the need to recover fine model details by using a higher-resolution grid (smaller grid dimension), and the minimization of the computation time and resources required by using coarser grid resolution. In this study, we test the sensitivity of the inversion result to the resolution of the model grid was tested using a dataset covering central and northeast Botswana (Figure S7 and S8). This test was done using a coarse grid of 30 km, an intermediate grid of 15 km and a fine 10 km grid resolutions

We compare the model misfits and the required number of NLCG iterations for the convergence of the three different electrical models with varying resolutions (Table S2). From the results, the overall nRMS decreases with increasing horizontal grid resolution. Increasing the resolution of the grid from 30 km to twice as fine resolution of 15 km has a considerable improvement on the nRMS. Similarly, a further increase in the grid resolution of the model from 15 km to 10 km significantly improved the data fit, which is evident in the reduced nRMS. Figure S9 shows how the MT site nRMS values for all the components of the data (Z and T) compare for the three models per MT sites. The nRMS per site generally decreases with increasing model grid resolution. These results reveal that finer grid model resolution inversion aids better data fit and increase the confidence in the recovered model.

Table S2: Summary of the nRMS for the Model Grid Resolution Sensitivity Test

Model Grid Resolution	Overall nRMS	Number of NLCG Iteration
10 km × 10 km	2.392333	98
15 km × 15 km	3.115478	82
30 km × 30 km	4.067719	74

To further gain insight from how the electrical structures develop in the three different models, depth sections at representative depths in the subsurface were examined. A plan view of the depth sections at 19 km and 49 km from the three models are given in Figure S7 and Figure S8, respectively. From the results of the 19 km depth section, it is revealed that the electrical structures are narrower and less connected in the fine grid model of 10 km. As the model grid resolution becomes coarser (15 km and 30 km), the electrical structures become wider and more connected spatially. Deeper electrical structures are also affected by the reduction of the model grid resolution in similar ways, as shown in the depth sections from 49 km (Figure S8). Also, the finer model shows fine and smooth boundaries of the electrical structures. It is observed that conductive structures are more distinctive at deeper depth in the finer grid model (Figure S8). From these results, it is revealed that finer grid resolution aid the recovery of high-resolution electrical structure with smooth boundaries.

From the results of this sensitivity test, a choice of 10 km grid resolution, which is also the minimum interstation spacing in the data was made for the new nationwide 3-D electrical conductivity modelling in Botswana. This helps to recover a finer model and more realistic model with better data fit. This helps to increase the confidence in the recovered model, which has better data fit and fine spatial resolution.

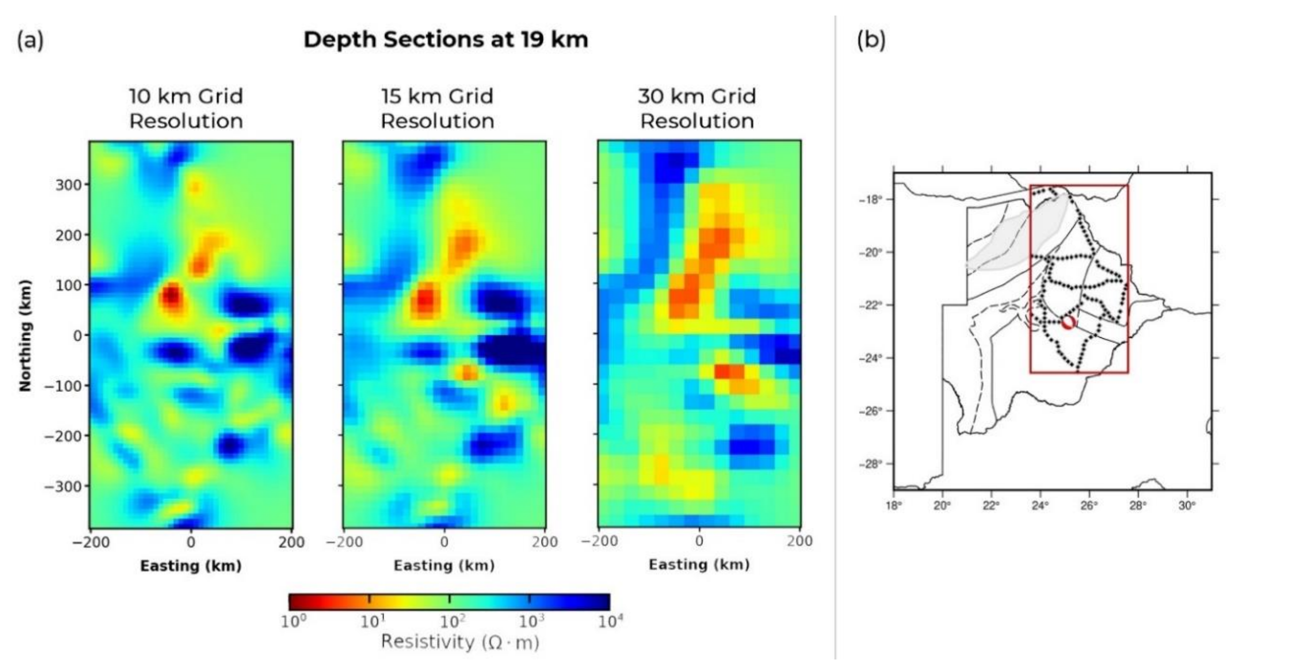

Figure S7: (a) Plan view of electrical conductivity model depth slices at 19 km derived for 10 km, 15 km, and 30 km grid resolution (b) Location Map. Red bounding box = location of models presented in (a).

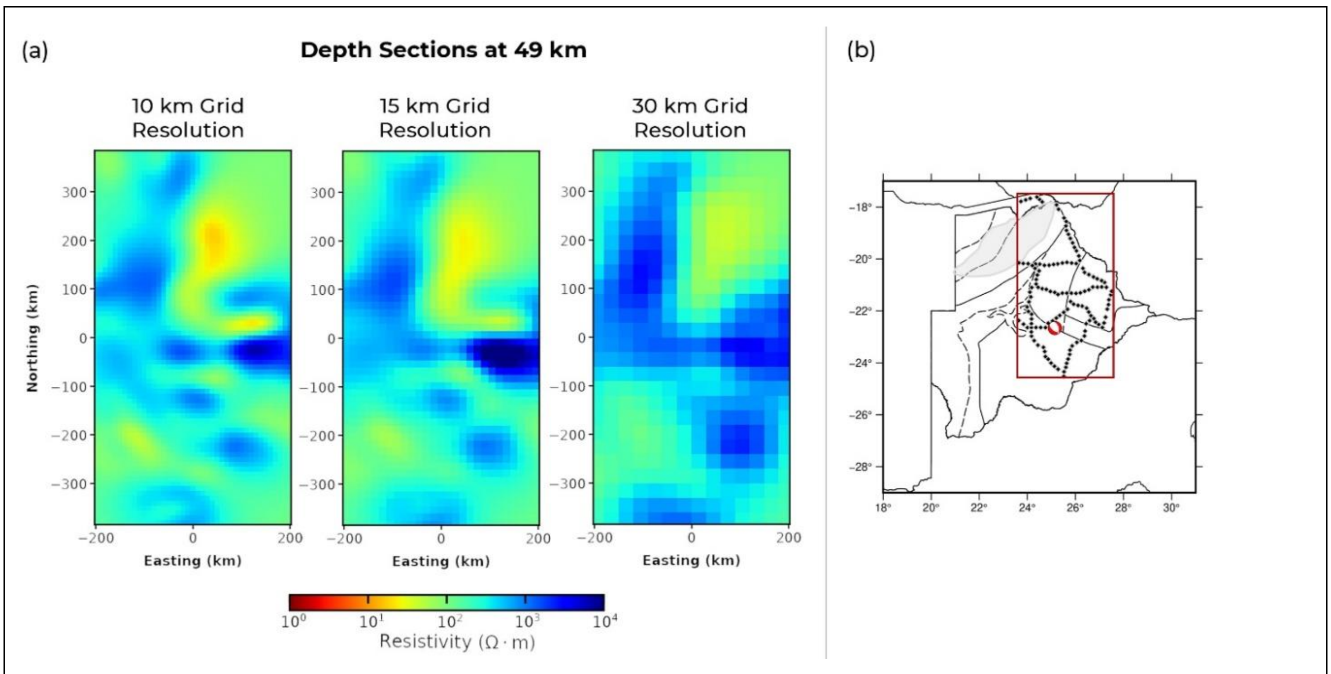

Figure S8: (a) Plan view of electrical conductivity model depth slices at 49 km derived for 10 km, 15 km, and 30 km grid resolution (b) Location Map. Red bounding box = location of models presented in (a).

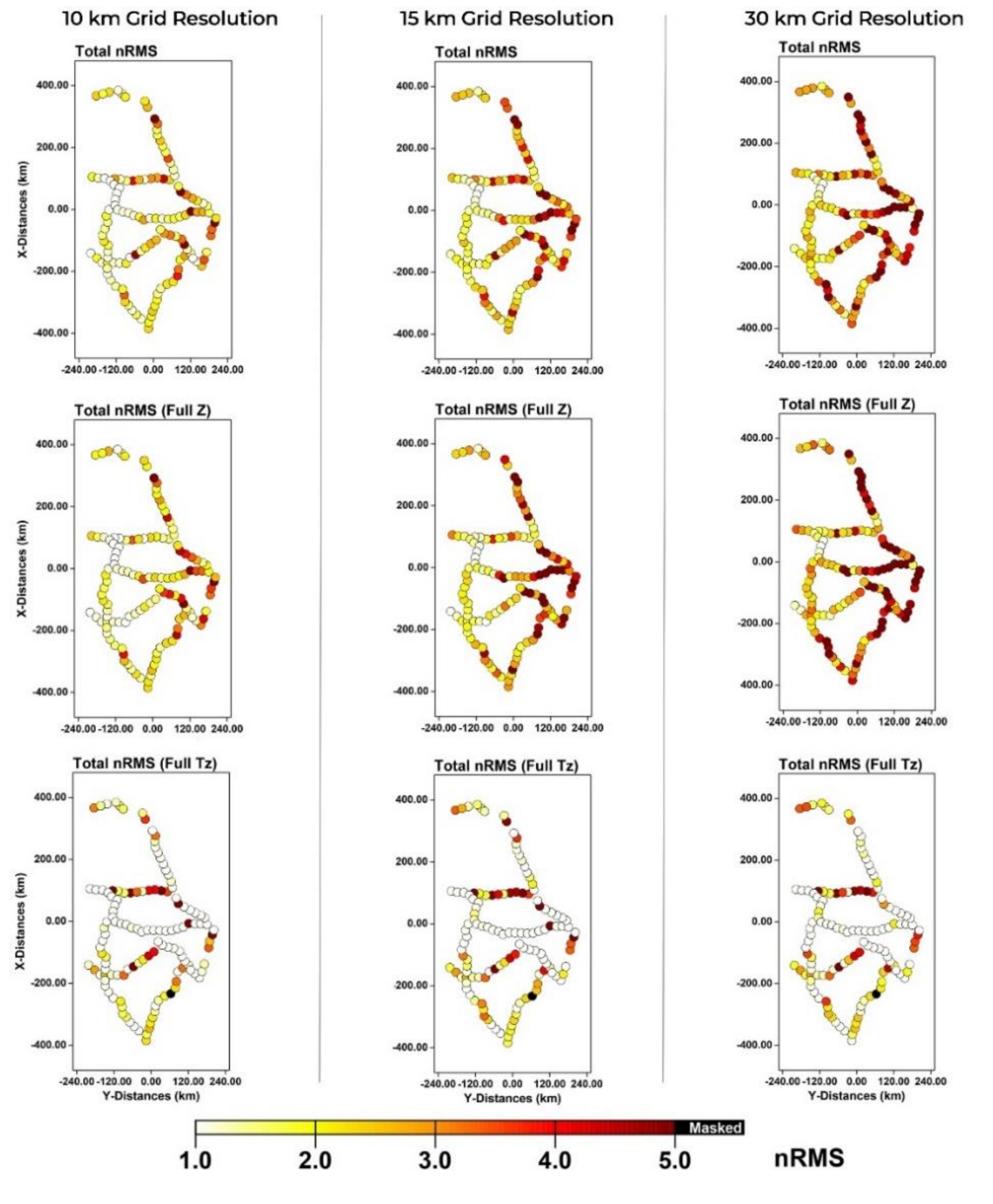

Figure S9: nRMS plot per station for impedance tensor and tipper data components derived for 10 km, 15 km, and 30 km model grid resolutions. The MT sites are represented in circles and the corresponding nRMS are indicated by the colour. Masked sites (shown in black colour) =no data.

2.3 Data Sensitivity of Conductive Structure

The description of this sensitivity test is described in the main text. Here, we repeat the description for the sake of completeness. A major uncertainty in our electrical modelling result was the highly conductive structures (1–10 Ωm) in the lower crust and upper mantle depths. A sensitivity test was carried out to verify the certainty of these high conductivity structures (1–10 Ωm) in the model if they are required in the model and data related. The test involved removing the conductive structures in the model and replacing them with the resistivity of the starting model (100 Ωm). The inversion is then restarted with the modified model. The resultant model was examined to see whether the high conductivity structures are returned in the model or not.

Figure S10 shows the results of the sensitivity test. From the results, it is observed that the high conductivity structures with resistivity values between 1 – 10 Ωm return back to the model after continued inversion of the modified model. This shows that the high conductive structures in the model are required and are data related.

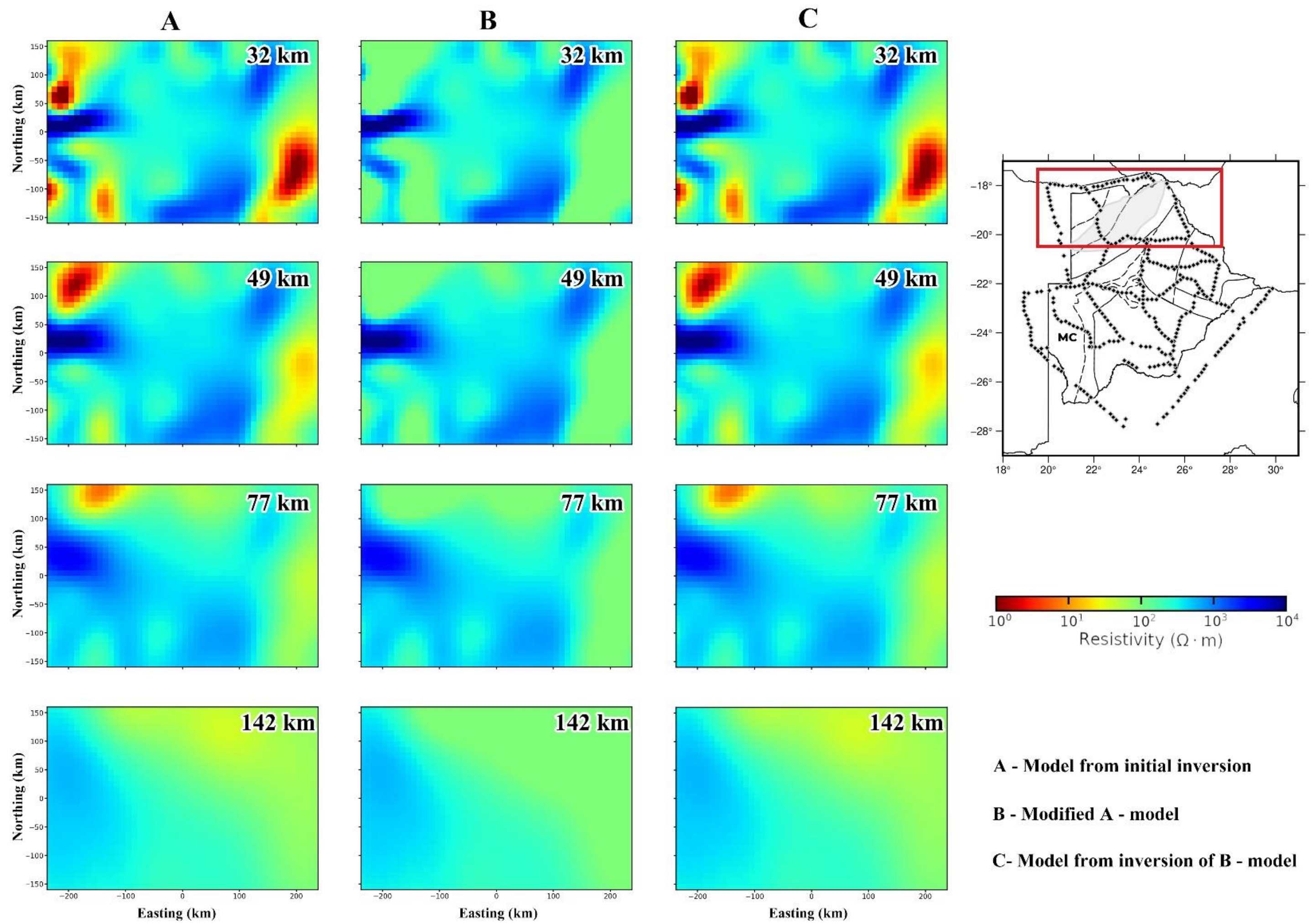

Figure S10: Plan view of electrical conductivity model depth slices at 32 km, 49 km, 77 km, and 142 km derived from model from initial inversion, modified model, and the model from the continued inversion of the modified model.

3 Data fit of the Final Model

3.1.1 Evaluation of Data Fit of the 3-D Nationwide Electrical Conductivity Model

To evaluate the result of the country-wide electrical conductivity model, nRMS analysis of the model was done to examine how it fits the measured MT data. Figure S11 shows the nRMS analysis between the measured MT data and the model-predicted data from the inversion as a function of the MT station for impedance tensor (Z) components, the VTFs components and all the components together. Figure S12 shows nRMS plot per station for each component of the impedance tensor and the tipper. From an examination of the nRMS for the components of the data used, the impedance tensor components have poorer nRMS (3.34) than the VTFs components (2.91). However, there are some sites with poor data fit across the whole dataset for both the impedance tensor and VTFs components, as shown in the total nRMS plots per site. Figure S13 and Figure S14 show the plot of measured and model-predicted responses for representative MT sites that are in close proximity to some of the major tectonic domains. The results show a good fit between the measured and model-predicted data across the whole periods for these representative sites.

From the inversion, the overall nRMS of the nationwide electrical conductivity model is 3.22 after 126 NLCG iterations. The overall nRMS is below the set error floors of 5% used in the inversion process, which is considered good for the model. This error is considered good for a comprehensive dataset in terms of spatial coverage and range of period as this.

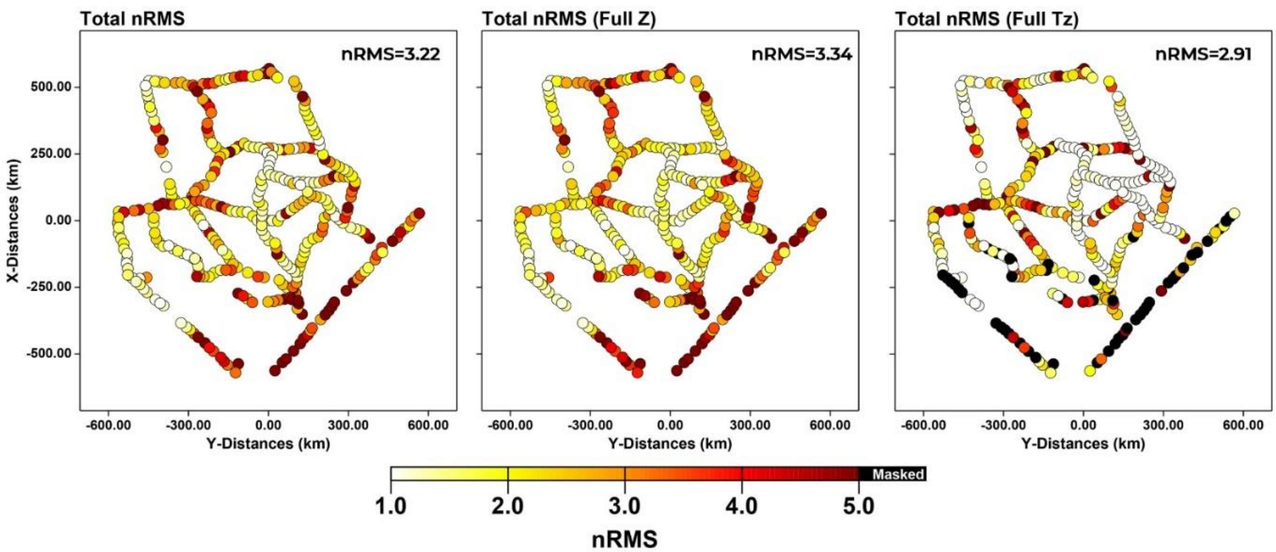

Figure S11: nRMS plot per station for all components of the MT data, impedance (Z) and VTFs. The MT sites are represented in circles, and the corresponding nRMS are indicated by the colour. Masked sites (shown in black colour) = no data.

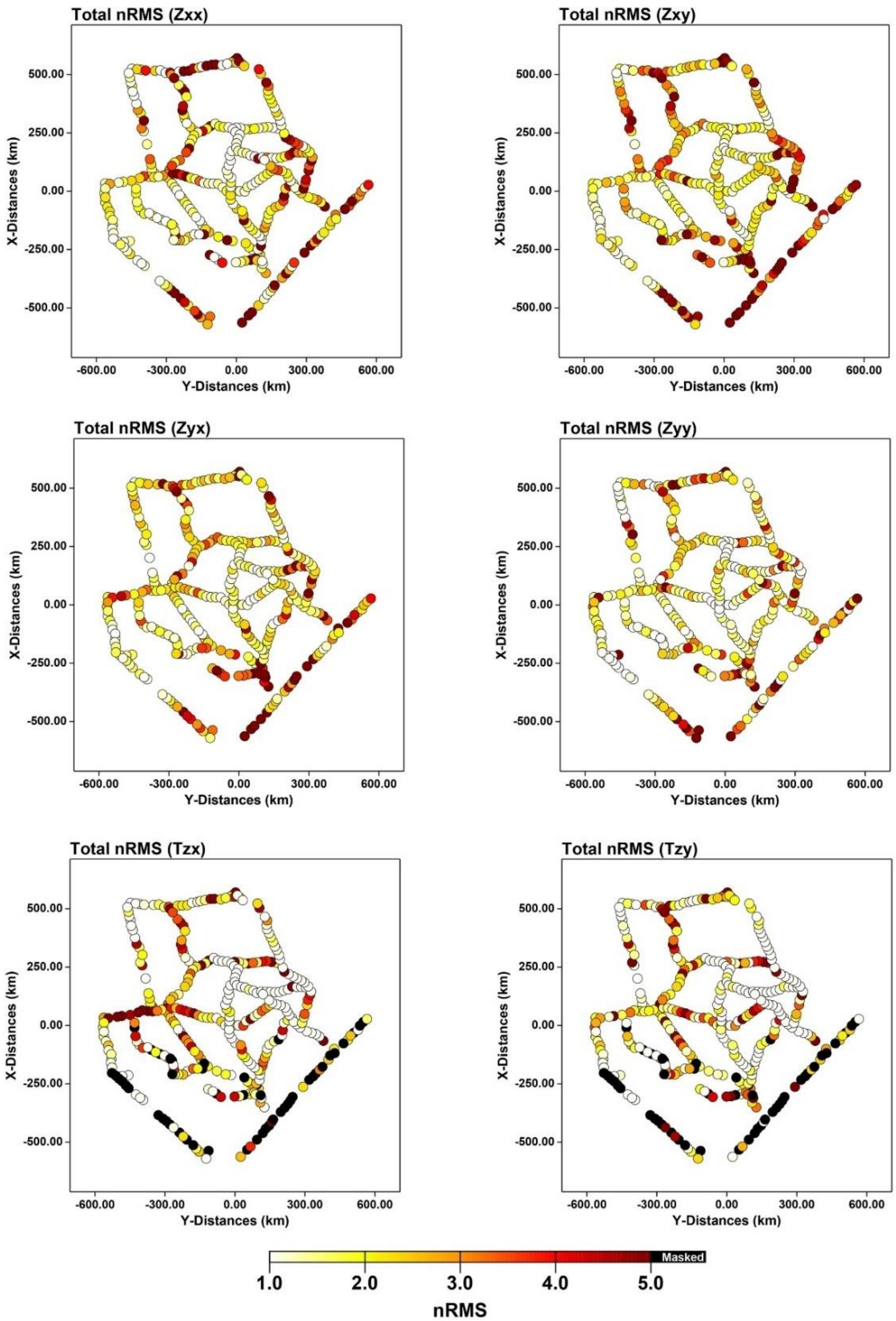

Figure S12: nRMS plot per station for each component of the impedance tensor and VTFs for the 3-D nationwide electrical model of Botswana. The MT sites are represented in circles and the corresponding nRMS are indicated by the colour. Masked (shown in black colour) = no data.

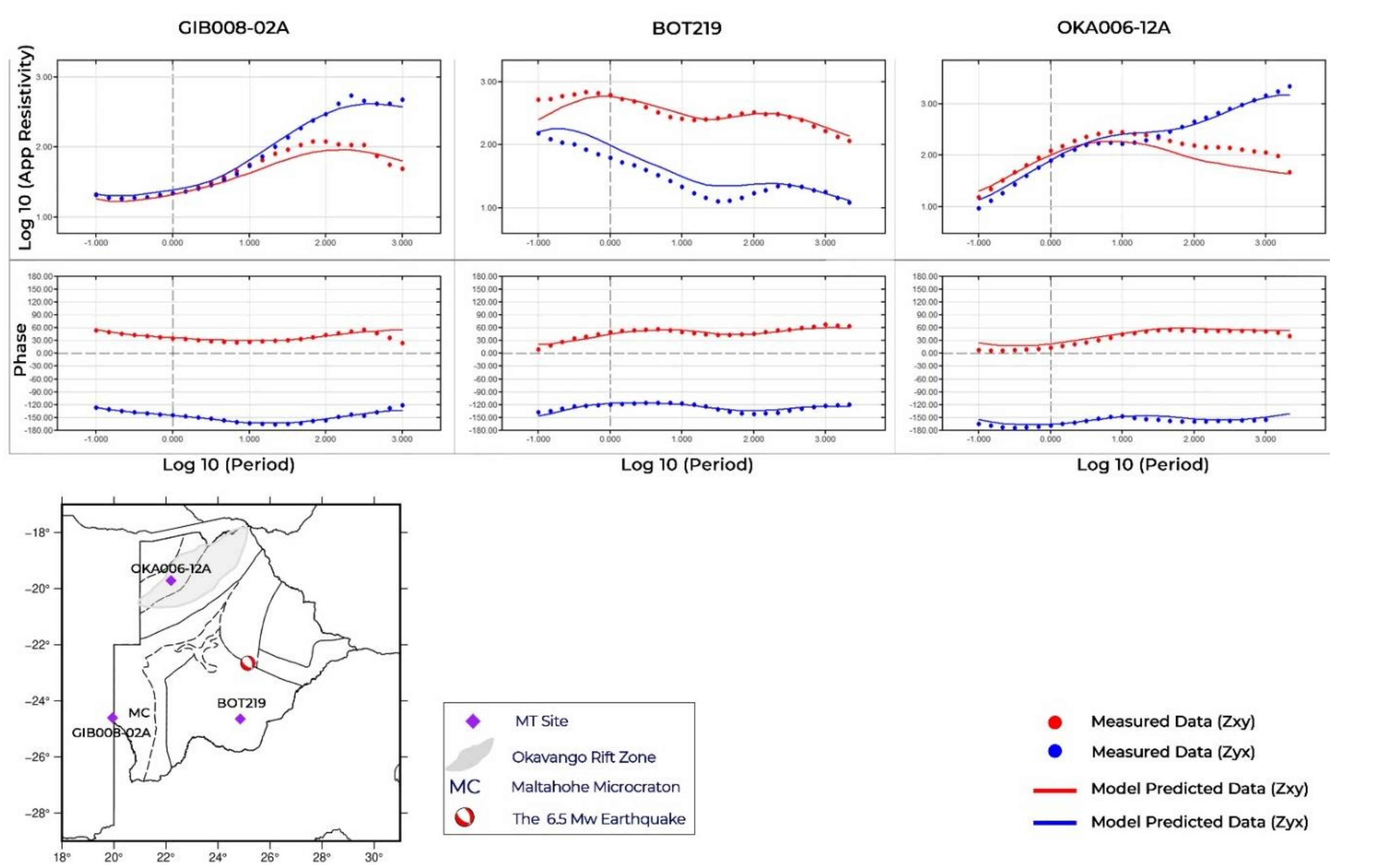

Figure S13: Observed and predicted responses for three representative MT Sites. Location map shows the MT sites analyzed.

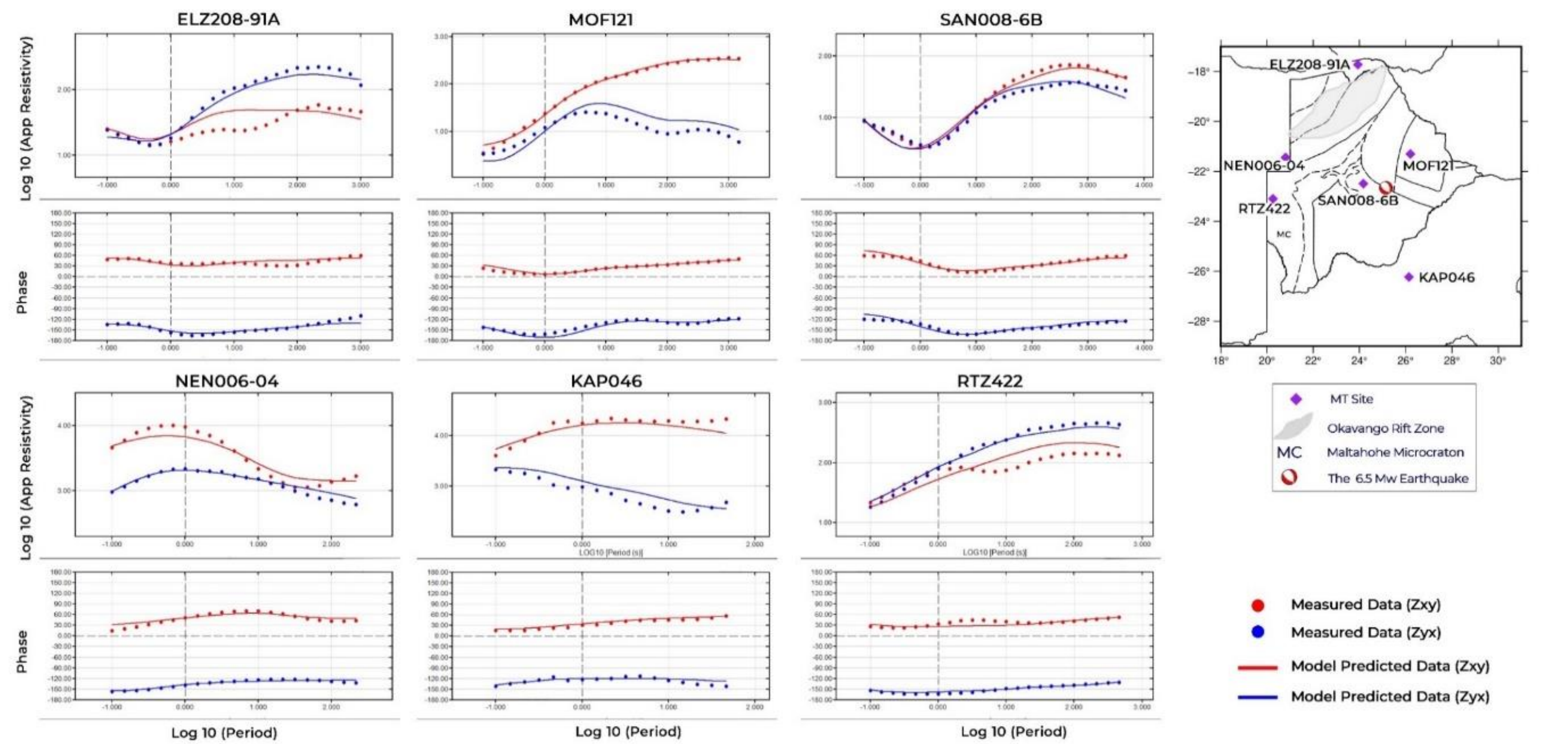

Figure S14: Observed and predicted responses for six representative MT Sites. Location maps shows the MT sites analyzed.